Economic Geology, v. 100, pp. 979–1003

Geology, Mineralization, Alteration, and Structural Evolution of the El Teniente Porphyry Cu-Mo Deposit

James Cannell,[†,*] David R. Cooke,

Centre for Excellence in Ore Deposits, University of Tasmania, Private Bag 79, Hobart, Tasmania 7001, Australia

John L. Walshe,

CSIRO Division of Exploration and Mining, 26 Dick Perry Ave., Kensington, Perth, Western Australia 6151, Australia

and Holly Stein

AIRIE Program, Department of Geosciences, Colorado State University, Fort Collins, Colorado, 80523-1482, and Geological Survey of Norway, Leiv Eirikssons vei 39, 7491 Trondheim, Norway

Abstract

El Teniente is a typical porphyry Cu-Mo deposit—in terms of its alteration and sulfide assemblage zonation, association with felsic intrusions, and predominance of quartz vein-hosted copper mineralization. It is anomalous in size, with >94 million metric tons (Mt) of contained fine copper making it the world's largest known porphyry Cu deposit. There is an intimate spatial and temporal association between all stages of mineralization and latest Miocene to early Pliocene felsic intrusions at Teniente.

Most of the copper was emplaced during the late magmatic stage (5.9–4.9 Ma), contemporaneously with intrusion of the dacite porphyry dike and dacite pipes into a mafic to intermediate sill-stock complex. Mineralization of the late magmatic stage is mainly hosted by a quartz-anhydrite–dominated stockwork associated with K-feldspar alteration in the dacites and Na-K-feldspar, biotite, and propylitic alteration of the mafic intrusive package. Minor copper-mineralized hydrothermal biotite-cemented breccias formed at this time. The late magmatic stage was followed by two stages of mineralized phyllic alteration, referred to as the principal hydrothermal (4.9–4.8 Ma) and late hydrothermal (4.8–4.4 Ma) stages, during which thicker, Cu-rich veins were emplaced. A 1,200-m-wide breccia pipe, the Braden Breccia, formed during the late hydrothermal stage and appears to have destroyed a large amount of ore from the center of the deposit.

The late magmatic and principal hydrothermal vein stages have predominantly concentric and radial vein orientations centered on the Braden Pipe. Most of the concentric veins are shallowly dipping, whereas the radial veins are subvertical. We present a model in which vein distributions were controlled by the local stress regime generated by the intrusion of a large, deep magma chamber that is interpreted to be the source of the dacites, the Braden Pipe, and ultimately, the copper and molybdenum mineralization. The late hydrothermal veins are steeply inward dipping and concentric to the Braden Pipe. In contrast to the late magmatic and principal hydrothermal vein stages, radial veins and shallow-dipping concentric veins are rare, consistent with formation during a stage of subsidence due to relaxation of intrusion-induced stresses. Resurgence of the magma chamber reactivated the steep concentric structures in a reverse sense, and a build up of magmatic and/or fluid pressure resulted in explosive brecciation and fluidization, producing the Braden Pipe. A predominantly late set of northeast-trending faults, associated with movements on the district-scale Teniente fault zone, is the only evidence for far-field stresses exceeding local stresses in the deposit.

Introduction

The El Teniente Cu-Mo porphyry deposit is located in the Andean Cordillera in the central Chile porphyry belt (Fig. 1). Central Chile is one of the world's most richly endowed copper provinces, with more than 180 million metric tons (Mt) of copper identified in five late Miocene-Pliocene porphyry Cu deposits (Fig. 1). El Teniente, owned by CODELCO, is the world's largest underground copper mine, containing 12.4 billion metric tons (Gt) at 0.62 percent Cu (current resource plus past production totals 94.4 Mt of Cu; Camus, 2002) and 7.8 Gt at 0.018 percent Mo (1.4 Mt of pure Mo).

Recently, Skewes et al. (2002) argued that El Teniente should not be considered a porphyry Cu deposit but rather a "breccia deposit" in keeping with the other large Miocene copper deposits of the central Chile belt (Los Pelambres, Atkinson et al., 1996; and Río Blanco, Serrano et al., 1996). Skewes et al. (2002) documented a variety of magmatic-hydrothermal breccia pipes interpreted to have formed over several million years that, together with abundant fine biotite veinlets, host the majority of the copper in the deposit. According to Skewes et al. (2002) the oldest mineralized biotite breccias and associated alteration formed before and after the 7 Ma Sewell Tonalite. They also argued that the dacite porphyry had a late to postmineralization timing, either removing preexisting copper mineralization or remobilizing it into a stockwork.

In this paper we document and interpret the geologic history, mineralization, alteration, geochronology, and structural framework of El Teniente. We have based the study on logging of 20 km of drill core, combined with petrography from

[†] Corresponding author: e-mail, j_cann@yahoo.com

[*] Current address: Lane Xang Minerals Limited, Sepon Copper Project, Laos.

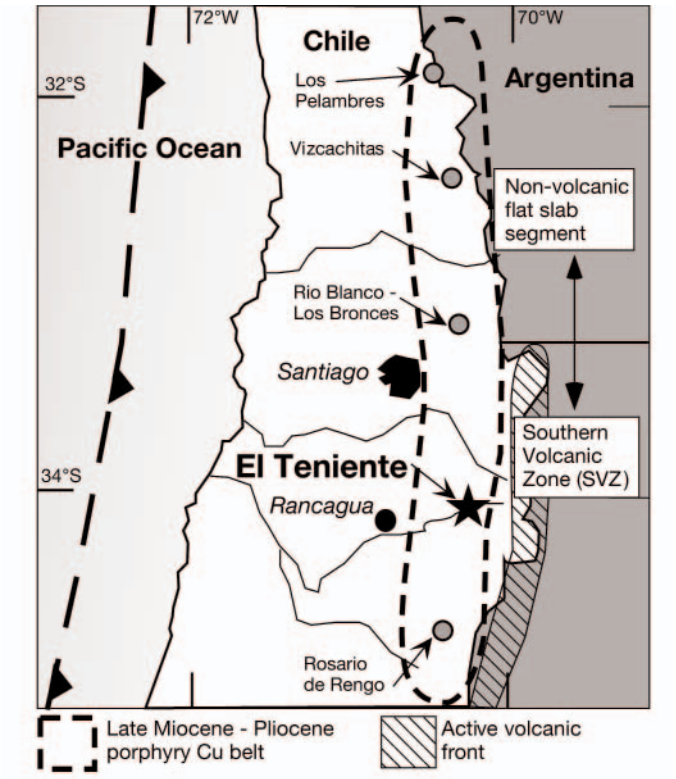

FIG. 1. Locality map—El Teniente is located in the central Chilean late Miocene-Pliocene porphyry-Cu belt. Also shown is the approximate boundary between the Southern volcanic zone (SVZ) and the nonvolcanic flat-slab segment (modified from Serrano et al, 1996; Camus, 2002). Other giant porphyry copper-molybdenum deposits occur at Los Pelambres and Río Blanco-Los Bronces, and copper-molybdenum porphyry prospects occur at Vizcachitas and Rosario de Rengo.

approximately 200 thin sections. Logged drill holes were chosen mainly from three cross sections with additional drill holes selected to gain information from as much of the deposit as possible. We provide a temporal analysis of the structural evolution of the deposit, based on a structural database compiled by mine geologists (4,337 vein orientation measurements from underground exposures). We provide evidence that supports the conventional porphyry Cu model constructed progressively by previous workers (Howell and Molloy, 1960; Camus, 1975; Cuadra, 1986). Apart from its extreme size, El Teniente shows many features typical of porphyry Cu deposits, and we argue that it should be classified as such. We use our results here to demonstrate how the shallow emplacement of a composite felsic intrusive complex has controlled the hydrothermal and structural evolution of El Teniente, in contrast to the mineralized breccia model of Skewes et al. (2002).

Geologic Setting

The mid-late Miocene Farellones Formation hosts El Teniente. It is a flat-lying sequence of arc-related volcanic and volcaniclastic rocks located trenchward of the current volcanic front (Fig. 1). The Farellones Formation is underlain by the Coya-Machali Formation (23–15 Ma; O. Rivera, 1999, unpub. for CODELCO; Godoy et al., 1999; Charrier et al., 2002), which formed in a tholeiitic arc setting overlying thin continental crust (Kay et al., 1999; Charrier et al., 2002). The contact between the two units is structural or locally unconformable (Thiele et al., 1991; Godoy et al, 1999). Charrier et al. (2002) suggested that deposition of the Coya-Machali Formation is related to crustal extension, and an increase in convergence rates between the Nazca and South American plates led to tectonic inversion, followed by deposition of the Farellones Formation.

The Coya-Machali and the Farellones Formations in the Teniente district were intruded by a series of calc-alkaline felsic to intermediate intrusions between 12 and 7 Ma. These are termed the Teniente plutonic complex, and include the Sewell Tonalite and/or diorite intrusive complex (dated between 8.9 and 7 Ma; Cuadra, 1986; S. Kay and A. Kurtz, 1995, unpub. report for CODELCO; Kurtz et al., 1997). The youngest intrusions known from the district occur within the Teniente deposit. They include the dacite and latite porphyries (5.67 ± 0.19–4.82 ± 0.09 Ma: Maksaev et al., 2004) and lamprophyre dikes (3.8–2.9 Ma: Cuadra, 1986; Maksaev et al., 2004).

Mapping by O. Rivera and M. Falcón (1998, unpub. report for CODELCO) identified four remnant volcanic centers with ages of 11 to 9 Ma in the Teniente district. They are associated with subvolcanic andesitic intrusions and lie on a northwest–north-northwest–trending lineament termed the Codegua fault (Fig. 2). This structural feature is apparent in local- to regional-scale aeromagnetic maps, but surface expressions are difficult to find. Based on the aeromagnetic data, the Codegua fault is interpreted to be a basin-bounding structure that has undergone significant vertical movement and has caused accumulation of volcanic debris to the south (P. Gow, pers. commun., 2000). Northwest-trending arc-transverse structures, such as the Codegua fault, have influenced the formation of Miocene volcanotectonic basins throughout central Chile (Rivera and Cembrano, 2000; Rivera and Falcón, 2000). These structures are believed to have formed due to reactivation of north-northwest–west-northwest–trending Mesozoic basement structures during the development of the Andean Cordillera (Rivera and Cembrano, 2000; Rivera and Falcón, 2000).

El Teniente is situated close to the intersection between the Codegua fault and the Teniente fault zone (Fig. 2). The Teniente fault zone is a 14-km-long zone of anastamosing faults trending northeast–east-northeast, which are associated with strongly developed unmineralized argillic alteration (Agua Amarga prospect: Camus, 1975; Cuadra, 1986; R. Floody and C. Huete, 1998, unpub. report for CODELCO).

Deposit Geology

Mine andesites

The principal host rocks at El Teniente are the mine andesites, traditionally grouped as part of the Farellones Formation (Fig. 3). The textural and geochemical features of the mine andesites have been obscured by widespread, pervasive, texturally destructive biotite alteration, and they have been interpreted in different ways by previous workers. Lindgren and Bastin (1922) described the host rocks as intrusive andesites, and Howell and Molloy (1960) described them as

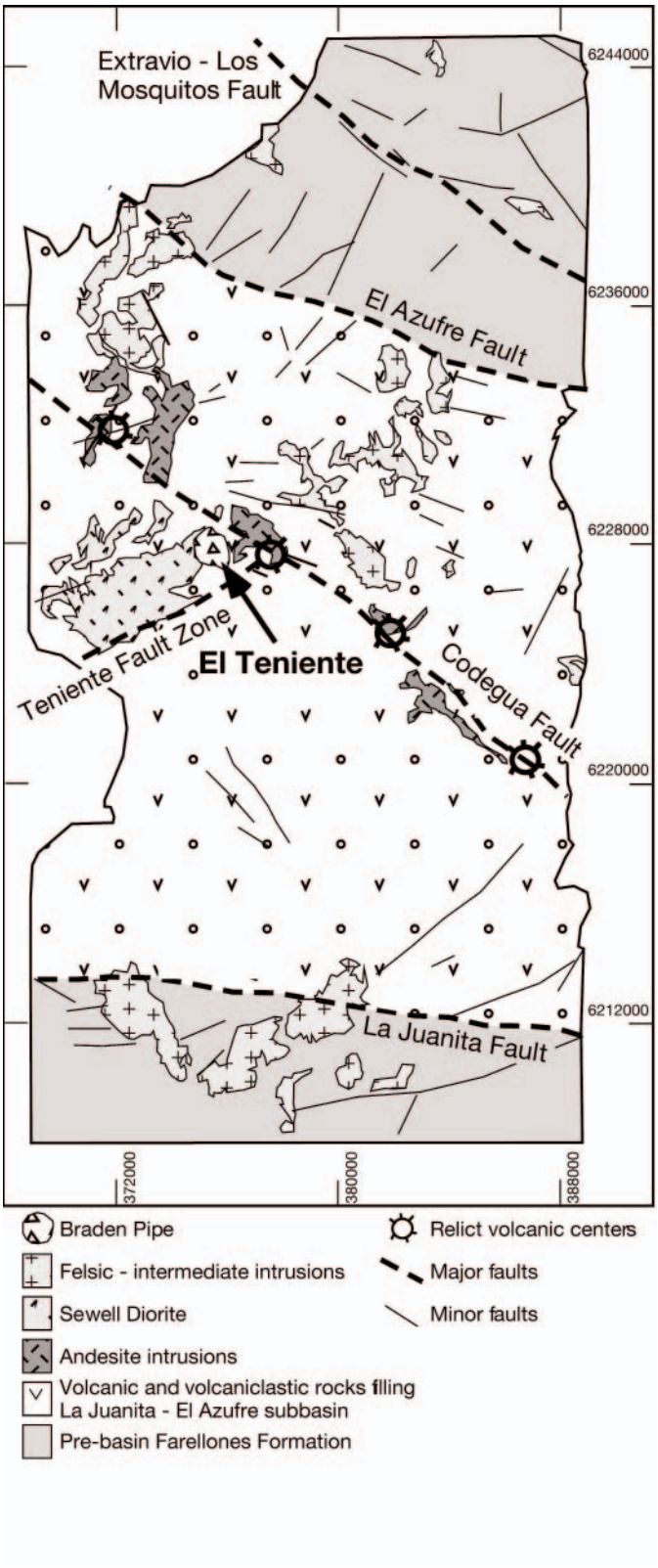

FIG. 2. Geology of the Teniente district. A northwest-trending lineament of relict eruptive centers occurs along the postulated Codegua fault within a volcano-sedimentary basin. El Teniente occurs close to the intersection of the Codegua fault with the northeast-trending Agua Amarga fault, part of the Teniente fault zone. Modified from O. Rivera and M. Falcón (1998, unpublished report for CODELCO).

thick, massive andesite flows of the Farellones Formation, with rare intercalated breccia lenses. A. Skewes (1998, 1999, unpuplished reports for CODELCO) and Skewes et al. (2002) described them as crystal-supported gabbroic intrusions, cut by a complex of biotite-matrix hydrothermal breccias.

Based on detailed core logging and thin section petrography we have reclassified the rock units (Table 1) and logged their occurrence in drill core in several cross sections through the deposit (e.g., Fig. 4). In agreement with Lindgren and Bastin (1922) and Skewes et al. (2002), we interpret the mine andesite package as a sill and stock complex containing crystal-supported, feldspar ± hornblende-phyric to aphanitic andesite sills (Fig. 5A). The sills have intruded andesitic lava flows (Fig. 5B) and volcaniclastic units (Fig. 5D) of the Farellones Formation. Microprobe analyses indicate that the plagioclase phenocrysts are strongly calcic (An_{46}–An_{92}, mostly between An_{60} and An_{85}: Skewes, 1997, 1998, unpuplished reports for CODELCO; Skewes et al., 2002; Cannell, 2004).

The distribution of the mine andesites in section 83 is shown in Figure 4. On the east side of the dacite porphyry, the andesite porphyry sill complex is the predominant host rock to mineralization below the 2,200-m level. The andesitic sill complex is at least 450 m thick in this section. Fine-grained andesite porphyry concordantly underlies a volcanic breccia zone on the east side of the dacite porphyry. Clasts of andesite porphyry in the volcanic breccia (Fig. 5D) suggest that the andesite porphyry unit is either partly extrusive or was uplifted and eroded after emplacement. The presence of amygdales and rare domains of intermingled sediment and andesite on the upper margins of the fine-grained andesite porphyry (interpreted to be peperite) support a shallow intrusive origin for the igneous units. Based on textural and mineralogical similarities we correlate the andesite porphyry in the Teniente mine with mafic to intermediate subvolcanic rocks described and mapped to the east of Teniente (andesite intrusions in Fig. 2) and around the Agua Amarga prospect to the west of the mine (R. Morel and C. Spronhle, 1992, unpub. report for CODELCO; Skewes et al., 2002). The surrounding Farellones Formation consists of subhorizontal, predominantly fine-grained, undifferentiated volcaniclastic units, volcanic breccias (Fig. 5D), and coherent volcanic flows. On the western side of the dacite porphyry, the fine-grained andesite porphyry cuts the volcanic and/or volcaniclastic sequence discordantly. Apparently subvertical, subequigranular stocks intruded the sill complex on the periphery of the ore deposit. The host sequence is cut by vertical, thin, fine-grained, porphyritic andesite dikes and late-stage hydrothermal biotite-matrix breccias (up to 30-m apparent thickness; Fig. 5C; see below). In contrast to the conclusion of Skewes et al. (2002), the biotite breccias in section 83 are volumetrically minor (Fig. 4), and most of the wall rocks, although altered and veined, are not brecciated.

Nine samples of altered mine andesites were analyzed for their major and trace element compositions (Table 2). Altered mine andesites have SiO_2 contents between 46 and 57 wt percent (Table 2; Camus, 1975; Villalobos, 1975; Skewes et al., 2002) and trace element ratios that classify them geochemically as gabbro or diorite (Fig. 6, Table 2). However, due to the large extent of the Teniente alteration system (>4 × 3

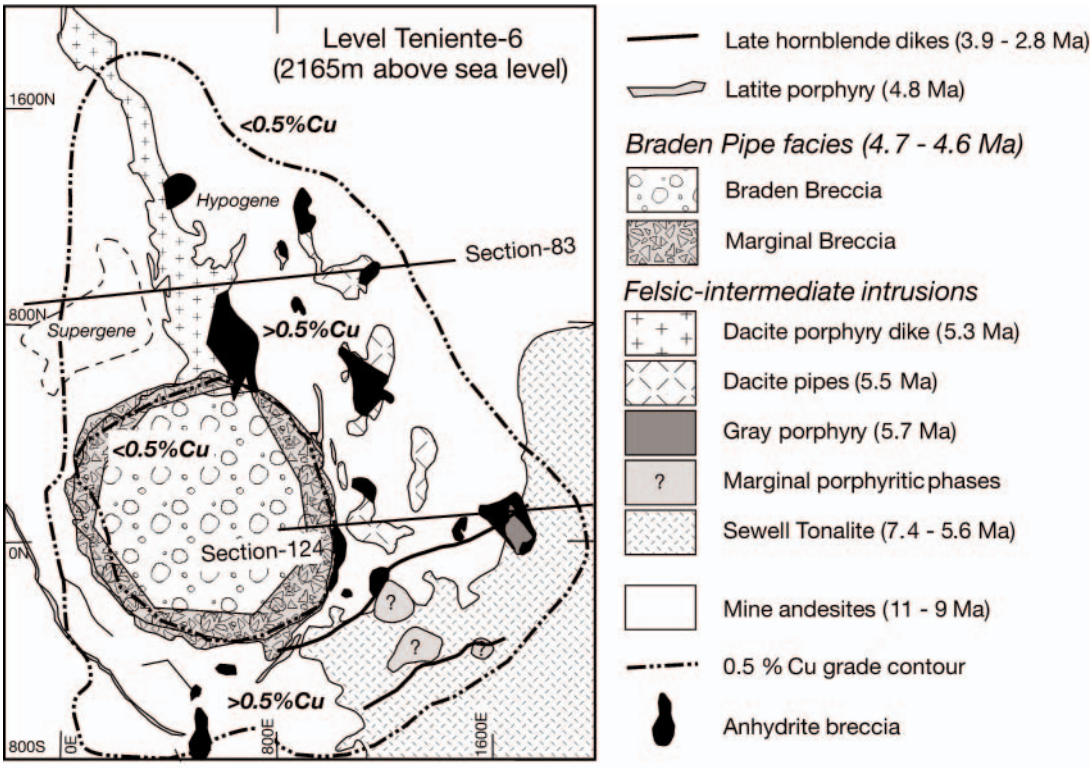

FIG. 3. Geology of Teniente level 6 (2,165 m), showing the locations of sections 83 and 124. This plan has been modified from the geologic data, based on underground mapping, contained in the mine database (data courtesy of CODELCO).

TABLE 1. Lithofacies of the Farellones Formation and Mine Andesite Sill and Stock Complex, El Teniente

Lithotype	Distribution/ occurrence	Features	Interpretation
Crystal-poor euhedral andesite unit	Rare; mainly occurs on west side of section 83	Porphyritic, 20 to 30% fine- to coarse-grained plagioclase phenocrysts and rarely preserved hornblende; fine groundmass, + amygdales	Coherent volcanic flow
Crystal-poor anhedral unit	Predominant unit above 2,200-m elevation in mine	Less coherent, subhedral to anhedral plagioclase crystals; fine-grained to aphanitic groundmass, occasionally with quartz grains and feldspar crystals	Volcaniclastic origin
Horizontal breccia zones	Thin horizontal units in volcaniclastic zones; abundant in section south of Braden Pipe	Contain abundant polylithic subrounded clasts up to tens of centimeters wide	Volcaniclastic breccias
Coarse-grained andesite porphyry	Stocks/sills; locally >450 m thick, sills up to 100 m thick	Porphyritic crystal rich (30–50% plagioclase phenocrysts) sub- to euhedral to equant plagioclase phenocrysts, coarse grained (>2 mm long phenocrysts), crystal- to groundmass-supported; rare hornblende crystals and amygdales; heterogeneous complex, variation in phenocryst size, and abundance	Sill/stock intrusive complex
Fine-grained andesite porphyry	Spatially associated and typically surrounding the coarse andesite porphyry unit	As above but phenocrysts <2 mm, up to 60% of rock; can be fine-grained equigranular; ± amygdales ± autobrecciated margins	Sill complex
Gabbro	One stock on far west side of section 83	Equigranular, coarse grained	Stock
Diorite Porphyry	Subvertical stocks and dikes <10 m wide	Medium- to coarse-grained, crystal rich, 40 to 70% equant to anhedral interlocking plagioclase phenocrysts; light gray	Stock and dikes
Andesite dikes	Subvertical dikes <5 m thick, sharp contacts	20 to 40% phenocrysts, coarse- to fine-grained phenocrysts (± polycrystalline aggregates) in a fine groundmass of interlocking/ aligned microliths	Dikes (low level of alteration suggests late timing)
Biotite Breccias	Subvertical breccia zones (one in section 83 is inclined 30°), typically <5 m (up to 30 m)	Composed of polylithic, andesitic to leucocratic clasts some of which are altered and veined; matrix composed of biotite, quartz, anhydrite, sulfides; can be well mineralized	Hydrothermal breccias associated with intrusion of the dacite

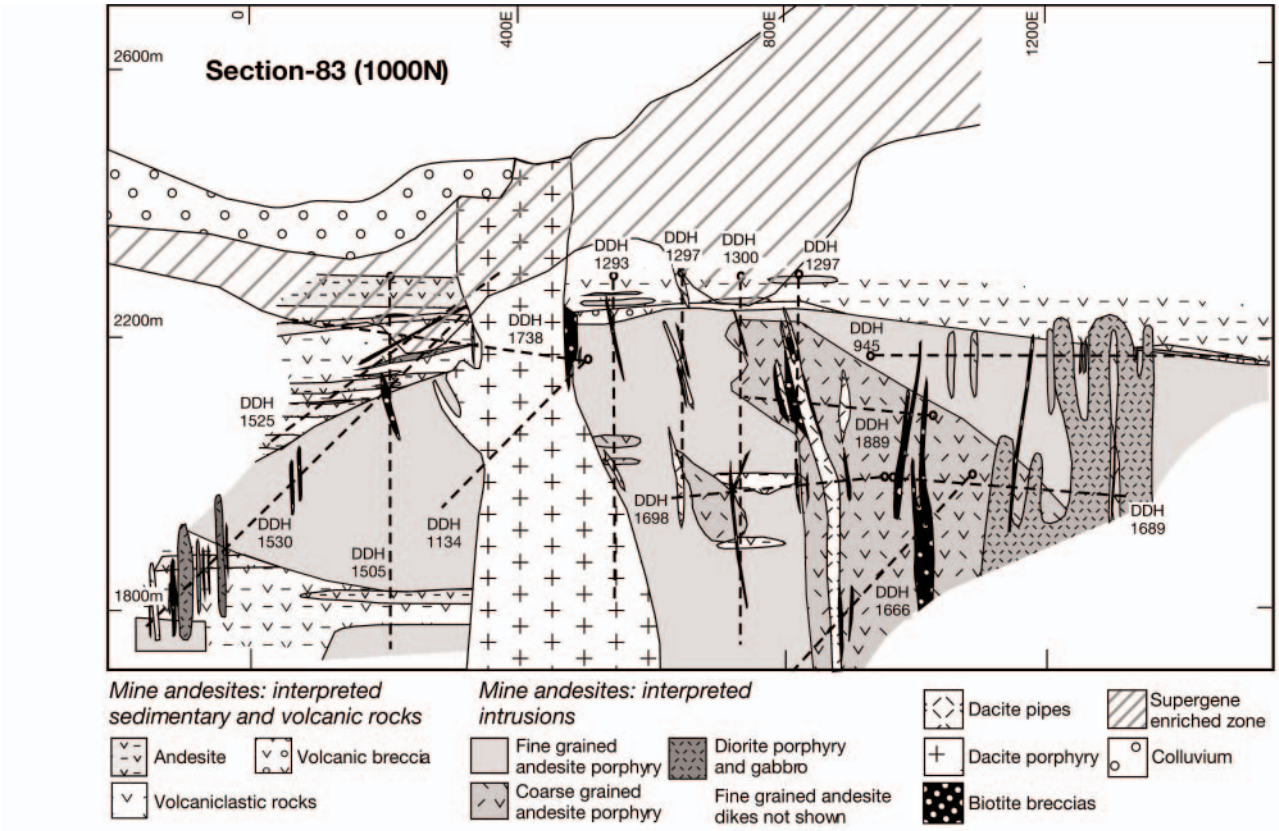

FIG. 4. Geologic cross section 83 (located at 1000N), showing the interpreted distribution of lithofacies of the mine andesite sill and stock complex and the biotite breccias, based on logging of 14 drill holes in this section (drill holes labeled as DDH 1293, etc.). A number of thin porphyritic andesite dikes cut the sequence but are too thin to be shown at this scale. The distribution of the felsic intrusions, supergene zone, and colluvium in this section was obtained from the mine database, courtesy of CODELCO, and is based on more drill holes than those indicated. The dashed line represents the limits of >0.5 percent Cu mineralized ore shell. Additional geologic cross sections are contained in Cannell (2004). In the supergene zone anhydrite has been dissolved and the feldspars are altered to kaolinite. Rock textures are mostly preserved in this zone.

km), no fresh rocks have been identified to date that are unambiguously equivalent to the Teniente mine andesites. The major elements (including K, Na, Ca and Si) are likely to have been mobile during the processes of potassic alteration, hence the primary mine andesite compositions are not known.

Felsic to intermediate intrusions and the Braden Pipe

A series of felsic to intermediate intrusions were emplaced into the andesitic host rocks (Table 3). The premineralization plagioclase-hornblende-phyric Sewell Tonalite (Fig. 3) is the oldest felsic to intermediate intrusion in the deposit (Table 3). Two textural varieties are identified (Camus, 1975; Guzman, 1991), an inner equigranular phaneritic phase and an outer porphyritic phase (Table 3). In section 124, the biotite-plagioclase-K-feldspar-phyric gray porphyry intruded the Sewell Tonalite (Table 3, Fig. 3). Thin, cylindrical to irregular felsic intrusions occur in the north and east of the deposit (Fig. 2). These were previously termed quartz diorite and/or tonalite apophyses (e.g., Camus, 1975; Cuadra, 1986), however based on their mineralogy and geochemistry (see below) in this study they are reclassified as dacite pipes.

U-Pb SHRIMP dating of zircons by Maksaev et al. (2002, 2004) has shown that the porphyritic phase of the Sewell Tonalite, the gray porphyry, and thedacite pipes have bimodal age distributions, with peaks at 6.46 ± 0.11 to 6.11 ± 0.13 and 5.67 ± 0.19 to 5.48 ± 0.19 Ma (Table 3). Maksaev et al. (2002) interpreted the older ages to be inherited from previously crystallized zircons and the younger ages to be the ages of final crystallization, whereas Maksaev et al. (2004) interpreted the older ages to be the intrusion ages and the younger ages to relate to hydrothermal activity.

The dacite pipes (5.50 ± 0.24 Ma: Table 3; Figs. 3, 4) and the dacite porphyry dike (5.28 ± 0.10 Ma: Table 3; Fig. 3) are plagioclase (±quartz, biotite) phyric porphyries with an aplitic groundmass. They are temporally and spatially related to Cu- and Mo- bearing veins and potassic alteration (Camus, 1975; Villalobos, 1975; Zúñiga, 1982; Guzman, 1991). Ossandón (1974) and Rojas (2002) have identified discrete intrusive phases of the dacite porphyry dike based on phenocryst sizes, abundances, proportions, and form (Table 3). K-feldspar is a rare phenocryst phase in all of the dacite intrusions but is locally abundant in the groundmass. Quartz phenocrysts are also uncommon in the dacites (typically <2%), but quartz is abundant in the groundmass (approx 20%). Rare primary (?) anhydrite occurs as a fine groundmass constituent. The dacites locally have igneous breccias, characterized by wallrock clasts in an igneous dacitic groundmass, at their contacts (Skewes et al., 2002).

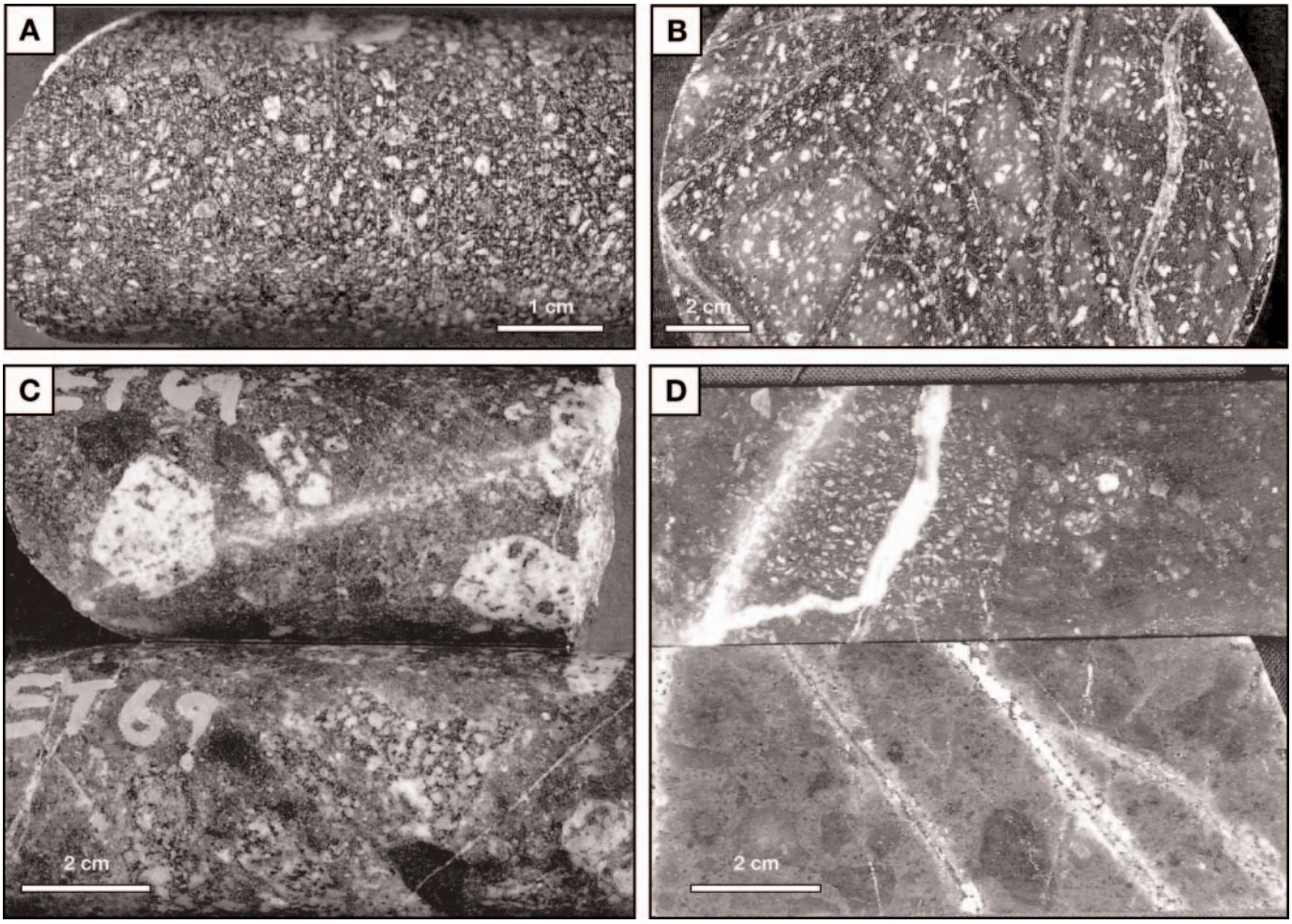

FIG. 5. Lithotypes of the mine andesite sill and stock complex. A. Coarse-grained, crystal-rich andesite porphyry, with >40 percent subhedral plagioclase phenocrysts. Crystal to groundmass supported (ET112A, DDH1698, 14.6 m). B. Coarse-grained, porphyritic crystal-poor andesite, euhedral to subhedral plagioclase phenocrysts, interpreted to be a coherent andesite flow (Ten, level 6). Late magmatic veins with dark-colored biotite halos cut the lighter colored, pervasive early magnetite alteration assemblage. C. Biotite breccia containing subrounded felsic and mafic clasts (ET69, DDH1689, 42.4 m). D. Volcaniclastic breccias. Top, monomictic breccia containing subangular andesite porphyry clasts in a secondary biotite-rich matrix (ET649, DDH1698, 18.9 m). Bottom, monomictic breccia composed of subangular dark- to light-gray aphanitic clasts, some with curviplanar edges, in a gray aphanitic matrix containing fine biotite-altered mafic crystals (ET786, DDH1409, 293.7 m).

The Braden Pipe is a massive, late to postmineralization breccia pipe with low copper grade that occurs in the center of the deposit. It has an inverted cone shape, is 1,200 m wide at surface, with 60º to 80º inward-dipping walls (R. Floody, 2000, unpub. report for CODELCO). A lower contact was intersected 1,400 m below surface in the deepest drill hole, which passes into an underlying latite stock. The Braden Pipe is made up of two principal breccia facies, the mineralized Marginal Breccia and the largely barren Braden Breccia (dated by K/Ar on sericitic clasts at 4.7 and 4.6 Ma, respectively: Cuadra, 1986).

The Marginal Breccia is a <1- to 60-m-thick monomictic, clast-supported breccia unit that occurs as a rim around the Braden Pipe (Fig. 3). This breccia has tourmaline-rich cement, with accessory sulfates, sulfides, and sulfosalts and is associated with local angular wall-rock clasts with phyllic (quartz, sericite, chlorite) alteration. The Braden Breccia occurs in the central part of the Braden Pipe and is a poorly sorted, polymictic breccia with a rock flour-matrix and both stratified and unstratified facies. The breccia contains abundant, subrounded to subangular, phyllic-altered wall-rock fragments that contain truncated veins. Clasts of the Marginal Breccia are scarce within the Braden Breccia (R. Floody, 2000, unpub. report for CODELCO), suggesting that the original spatial extent of the Marginal Breccia was probably similar to its present day distribution.

Plagioclase-phyric latite dikes are the youngest altered intrusions in the deposit, dated at 4.8 Ma (Table 3). They are sericitized and occur as northwest- to west-trending dikes or as ring dikes <15 m thick that occur concentrically around the Braden Pipe (Cuadra, 1986). Pebble dikes, typically <2 m wide, containing rounded sericitized clasts also occur as incomplete ring dikes around the Braden Pipe. The youngest known intrusions in the deposit, and in the Teniente district, are thin northeast-trending lamprophyre dikes (3.8–2.9Ma: Table 3).

TABLE 2. Whole-Rock Geochemistry of the Mine Andesites

	Coarse andesite porphyry			Fine andesite porphyry				Gabbro	Andesite dike
	ET765 DDH1689, 272.8 m	ET671 DDH1306, 208.2 m	ET640 DDH1565, 451.6 m	ET742 DDH1314, 33.8 m	ET777 DDH1981, 221.0 m	ET407 DDH1423, 506.6 m	ET756 DDH1317, 12.2 m	ET768 DDH1530, 655 m	ET263 DDH1529, 195.1 m
SiO_2 (wt %)	49.3	46.22	51.03	50.23	53.18	54.59	53.46	50.91	53.58
TiO_2	0.98	1.17	1.26	1.11	1.02	0.93	1.04	0.96	1.05
Al_2O_3	18.62	20.71	20.18	19.26	17.31	17.8	17.84	18.08	18.58
Fe_2O_3	6.27	6.23	6.22	8.54	9.5	8.83	5.19	10.13	7.9
MnO	0.05	0.04	0.06	0.05	0.08	0.06	0.03	0.16	0.06
MgO	6.42	4.5	4.16	4.69	5.5	3.58	5.39	6.02	3.93
CaO	7.12	7.2	7.54	6.88	6.5	5.86	5.98	7.49	6.98
K_2O	3.76	3.42	2.39	2.41	1.85	2.3	3.49	2.67	1.23
Na_2O	2.31	4.38	3.11	2.82	1.95	3.34	2.93	1.44	2.65
P_2O_5	0.2	0.23	0.27	0.25	0.22	0.22	0.24	0.18	0.22
LOI	4.74	5.07	3.14	3.44	2.87	2.66	4.19	2.15	3.74
Total	99.77	99.17	99.36	99.68	99.98	100.17	99.78	100.19	99.92
Ti (ppm)	22541	20503	14328	14448	11091	13789	20923	16007	7374
P	873	1004	1178	1091	960	960	1047	786	960
Cr	97	38	24	15	103	6	107	151	8
Ni	47	25	17	17	45	8	42	59	8
Rb	173	175	103	139	103	121	204	131	74
Sr	425	491	528	453	358	523	471	351	480
Ba	291	346	307	83	142	269	147	175	114
Sc	30	34	33	30	27	23	31	31	30
V	332	332	372	274	240	232	291	279	278
Nb	2	2	3	2	4	3	4	2	3
Zr	65	70	95	90	140	96	137	95	84
Th	2	2	3	2	5	3	4	4	2
Y	15	16	18	22	19	18	19	16	18
La	11	10	10	6	12	16	12	7	7
Ce	25	28	25	20	31	25	30	14	18
Nd	15	14	14	13	18	14	17	9	12
Cu	7085	15600	4526	395	278	149	525	125	1976
Zn	50	48	52	52	58	53	26	68	48
Mo	25	94	12	3	2	3	1	2	3
Pb	3	10	4	4	3	4	3	2	5

Notes: Samples were analyzed by X-ray fluorescence (XRF) at the University of Tasmania; total iron reported as Fe_2O_3

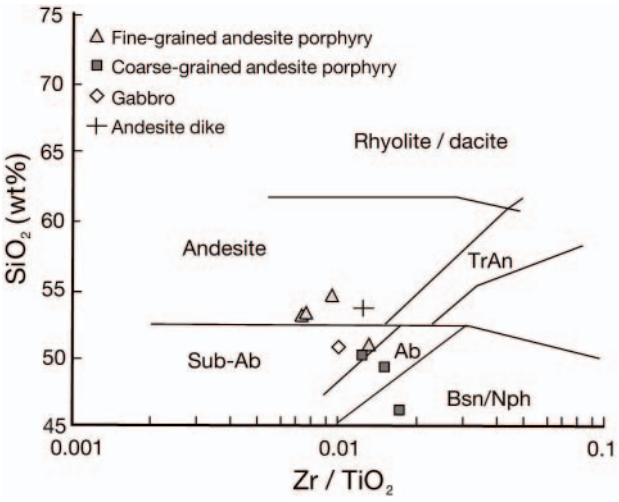

FIG. 6. Zr/TiO_2 vs. SiO_2 plot for least altered El Teniente mine andesites, showing the compositional fields of Winchester and Floyd (1978). The coarse-grained andesite porphyries and the gabbro are more mafic than the fine-grained andesite porphyries and the andesite dike. Abbreviations: Ab = alkali basalt, Bsn/Nph = basanite, nephelinite, TrAn = trachyandesite.

The dacite porphyry, dacite pipes, and latite dikes are all geochemically similar, classified as calc-alkaline dacites (61–68 wt % SiO_2: A. Skewes, 1998, 2000, upub. reports for CODELCO; Rojas, 2002; Skewes et al., 2002; Table 4), although data for dacite pipes from Villalobos (1975) span an SiO_2 range from 50 to 67 wt percent. The Sewell Tonalite samples vary from 60 to 66 wt percent SiO_2 (Guzman, 1991; Reich, 2000; Table 4). There is no consistent trend to more felsic or mafic compositions through time. A single analysis of altered gray porphyry indicates 51 wt percent SiO_2 (Table 4), consistent with a basaltic composition. The sample contains abundant volatile components due to hydrothermal alteration (loss on ignition of 11 wt %), and it is possible that SiO_2 removal occurred during potassic alteration, producing the anomalously low silica content.

Vein and Alteration Paragenesis

Based on our detailed observations throughout the deposit, copper and molybdenum mineralization at El Teniente is hosted mostly within a vein stockwork in the mine andesites and dacite intrusions. This contrasts with Skewes et al. (2002) who concluded that mineralization is predom-

TABLE 3. Petrography and Geochronology of Felsic to Intermediate Intrusions, El Teniente

Intrusion	Subtype	Location	Mineralogy	Texture	Age	References[1]
Sewell Tonalite	Equigranular	Stock in southeast corner of deposit	Plagioclase, hornblende, biotite, K-feldspar, quartz, sericite, chlorite, epidote	Equigranular	7.4 ± 1.0 to 7.1 ± 1.5 Ma (K/Ar, Cuadra, 1986)	Sewell diorite/ tonalite of Camus (1975), Faunes (1981), Guzman (1991), Kurtz et al. (1997)
	Porphyritic	Outer carapace to stock	Plagioclase, biotite, K-feldspar, quartz, sericite, chlorite, anhydrite	Porphyritic, 30 to 50% phenocrysts, aplitic groundmass	6.15 ± 0.16 and 5.59 ± 0.17 Ma (SHRIMP U-Pb on zircon, Maksaev et al., 2004)	
Gray porphyry		Intruded the Sewell Tonalite near its contact with mine andesites	Plagioclase, biotite, K-feldspar (perthite), anhydrite	Porphyritic, inequigranular groundmass	6.46 ± 0.11 and 5.67 ± 0.19 Ma (SHRIMP U-Pb on zircon; Maksaev et al., 2004) 5.1–6.0 Ma (K/Ar on biotite; Cuadra, 1992).	Cuadra (1992), Skewes et al. (2002)
Dacite pipes		Various (>6) pipes east of dacite porphyry. also has intruded Sewell Diorite along contacts?	Plagioclase ($An_{16–0}$), quartz, biotite phenocrysts in quartz-plagioclase-K-feldspar, groundmass	Porphyritic, 30 to 50% phenocrysts, groundmass is aplitic (<0.12 mm), to coarse grained (up to 0.5 mm)	6.28 ± 0.16 and 5.50 ± 0.24 Ma, 6.11 ± 0.13 and 5.48 ± 0.19 Ma (SHRIMP U-Pb on zircon; Maksaev et al., 2004)	Quartz diorite/ tonalite apophyses of Villalobos (1975), Camus (1975), Guzman (1991),
Dacite porphyry	Euhedral	Northern end of 1,500- × 200-m Dacite dike	Plagioclase ($An_{7–39}$), quartz, biotite phenocrysts in quartz-plagioclase-K-feldspar, groundmass	Euhedral phenocrysts, aplitic groundmass	5.28 ± 0.1 Ma (SHRIMP U-Pb on zircon; Maksaev et al., 2004) 4.7–4.5 Ma (K/Ar on biotite, Cuadra, 1986, 1992)	Ossandon (1974), Skewes et al. (2002), Rojas (2002)
	Subhedral	Central portion of Dacite dike		Subhedral phenocrysts, coarse groundmass		
	Igneous breccia	Contacts of all intrusive units above	Plagioclase, K-feldspar, biotite, quartz phenocrysts in quartz-feldspar-biotite groundmass	Wall-rock xenoliths <20%	Undated	Ossandon (1974), Rojas (2002)
Latite dikes		Concentric to Braden Pipe and northeast-trending thin dikes	Plagioclase ($An_{30–70}$), quartz, biotite phenocrysts in quartz-plagioclase-K-feldspar groundmass, sericitized	Porphyritic, 30 to 50% phenocrysts, very fine aplitic groundmass (<0.02 mm)	4.82 ± 0.09 Ma, (SHRIMP U-Pb on zircon; Maksaev et al., 2004) 5.3 (± 0.7)–4.8 (± 0.6) Ma (K/Ar on biotite, sericite, plagioclase; P. Cuadra, 1992, unpub. report for CODELCO)	Riveros (1989)
Lamprophyre dikes		Northeast-trending thin dikes	Hornblende, pyroxene, olivine, plagioclase	Fine-grained, porphyritic	3.85 ± 0.18 Ma (Ar^{40}/Ar^{39} on hornblende; Maksaev et al., 2004) 3.8 and 2.9 Ma (K/Ar: Cuadra, 1986)	Cuadra (1986)

[1] Table supplemented with information from the following unpublished reports for CODELCO: J. Ojeda, E. Hernandez, G. Ossandon and A. Enrione (1980); P. Cuadra (1992); A. Skewes (1997)

inantly breccia hosted. The 0.5 percent Cu contour in the Teniente level 6 outlines a wedge-shaped zone approximately 2.5 km long, 1.8 km wide (Fig. 3) and more than 800 m deep, with high-grade hypogene zones (>1.2% Cu, for 100s of meters) localized around intrusive centers (e.g., Esmerelda, sub-6). High grades also occur in the supergene zone, which locally extends down deeper around the dacite porphyry due to higher fracture intensities (Skewes et al., 2002). Higher molybdenum grades (>0.03% Mo) occur locally around the dacite intrusions and as a concentric ring around the Braden Pipe. There is a zoned distribution of sulfide minerals, with bornite occurring in the center of the deposit at the southern end of the dacite dike, passing outward to an intermediate annular domain characterized by chalcopyrite and finally to a pyrite (±pyrrhotite inclusions) domain occurring on the periphery (Camus, 1975; Cuadra, 1986, A. Arevalo and R. Floody, 1995, unpub. report for CODELCO).

Alteration and vein assemblages at El Teniente were divided by previous workers into four stages: the late magmatic,

TABLE 4. Geochemistry of the Felsic to Intermediate Intrusions at El Teniente

	Sewell Tonalite		Dacite porphyry			Dacite pipes			Gray porphyry	Latite porphyry			Lamprophyre	
	CE52 2 km S of Sewell	ET720 DDH 1463, 423.1 m	ET811 DDH 1291, 423.7 m	ET585 DDH 1525, 33.2 m	ET789 DDH 1505, 3.0 m	ET769 DDH 1297, 299.0 m	ET701 DDH 1889, 215.8 m	ET534 DDH 1676, 458.4 m	ET820 DDH 1680, 316.7 m	ET779 DDH 1981, 346.6 m	ET782 DDH 1079, 435.6 m	ET788 DDH 1068, 1012.9 m	ET452 DDH 855, 387.7 m	ET754 DDH 1314, 386.6 m
(wt %)														
SiO_2	59.9	61.12	65.47	67.62	64.66	66.14	1889	735	50.83	64.27	65.89	68.41	55.64	55.78
TiO_2	0.69	0.55	0.38	0.36	0.35	0.39	0.38	0.36	0.44	0.31	0.31	0.34	0.77	0.85
Al_2O_3	16.26	17.35	16.85	16.87	15.92	17.21	16.32	16.77	12.91	15.72	16.35	17.18	15.81	17.57
Fe_2O_3	7.54	2.61	0.68	0.89	0.63	1.88	1.04	1.31	3.76	1.78	2.1	1.34	4.88	5.64
MnO	0.15	0.03	0.01	0.01	0.01	0.01	0.02	0.01	0.03	0.07	0.03	0.01	0.11	0.08
MgO	2.78	1.87	0.93	0.98	0.89	0.84	1.23	1.03	1.94	0.74	0.78	0.8	3.12	3.71
CaO	3.4	3.6	3.21	1.35	3.31	3.12	3.82	2.94	8.56	4.89	2.03	2.71	6.67	5.86
K_2O	2.12	3.81	2.59	3.36	2.81	2.63	2.22	3.06	6.67	4.21	4.92	0.98	1.78	1.5
Na_2O	5.8	4.82	6.03	5.47	6.29	5.61	5.72	5.42	2.13	1.35	4.02	7.09	3.55	4.51
P_2O_5	0.18	0.34	0.14	0.13	0.14	0.13	0.14	0.14	0.21	0.12	0.13	0.13	0.25	0.28
LOI	1.04	3.74	3.29	2.15	4.17	2.07	4.7	2.33	10.99	6.66	3.47	1.04	7.17	4.27
Total	99.86	99.84	99.58	99.19	99.18	100.03	99.55	99.27	99.47	100.12	100.03	100.03	99.75	100.05
(ppm)														
Ti	12,709	22,841	15,527	20,143	16,846	15,767	13,309	18,345	39,987	25,239	29,495	5,875	10,671	8,993
P	786	1,484	611	567	611	567	611	611	916	524	567	567	1,091	1,222
Cr	39	15	6	7	6	5	10	6	18	5	4	4	76	73
Ni	14	10	4	5	3	1	6	4		2	2	3	41	45
Rb	54	203	65	84	61	51	85	72	209	160	140	32	42	28
Sr	407	608	773	486	611	771	627	782	536	228	331	711	736	956
Ba	464	524	628	657	485	712	417	854	692	564	742	238	376	414
Sc	13	8	5	5	4	3	5	4	9	3	4	3	14	14
V	175	103	66	75	72	63	79	72	203	56	52	66	141	148
Nb	3	3	2	3	2	3	2	2	3	2	2	2	3	4
Zr	114	107	91	91	85	93	94	94	78	99	87	100	125	133
Th	10	2	3	4	4	2	2	4	3	2	5	4	3	2
Y	12	8	4	4	4	4	5	3	9	4	3	4	9	8
La	12	16	13	11	9	12	14	11	37	15	13	7	14	15
Ce	25	37	30	24	29	30	27	26	72	29	27	16	37	41
Nd	14	18	14	12	13	14	12	12	33	11	12	8	21	23
Cu	107	1,136	1,387	5,215	5,806	623	2,460	4,625	10,100	18	1,426	6	46	47
Zn	123	36	17	28	27	17	41	32	34	35	26	34	102	76
Mo	78	12	8	52	38	2	161	47	255	1	22	4	2	2
Pb	52	3	6	5	12	4	6	9	9	4	2	16	12	7

Notes: Samples were analyzed by X-ray fluorescence (XRF) at the University of Tasmania; total iron reported as Fe_2O_3

principal hydrothermal, late hydrothermal, and "postuma" stages (Villalobos, 1975; Cuadra, 1986, Skewes et al., 2002). We have modified this basic paragenesis by adding a premineralization stage and by combining the postuma stage with the late hydrothermal stage (Table 3). We have also identified multiple vein generations within each of the main paragenetic stages, as described below.

Premineralization stage (type 1 veins)

A magnetite + quartz + anhydrite + actinolite + calcic plagioclase (An_{94}–An_{40}) ± epidote alteration assemblage predates mineralization at El Teniente (Skewes et al., 2002; Fig. 7A; Cannell, 2004). This assemblage varies from pervasive to vein controlled and occurs in association with magnetite veinlets (type 1a). Primary plagioclase phenocrysts have been partially replaced by fine disseminated magnetite (Fig. 7B). Remnants of this early magnetite alteration assemblage are preserved in andesitic units throughout the mine but are best preserved on the deposit margins.

A phyllic (tourmaline + sericite, chlorite, magnetite) alteration assemblage formed adjacent to the Sewell Tonalite. It is locally associated with thick, barren quartz veins (type 1b, Table 5). No copper or molybdenum mineralization was associated with this phyllic alteration.

Late magmatic stage (type 2 veins)

Emplacement of quartz-anhydrite-sulfide stockwork veins and extensive potassic alteration occurred during the late magmatic stage, synchronous with intrusion of the dacite. The relative proportion of copper introduced during the late magmatic stage (and the principal hydrothermal and late hydrothermal stages) was estimated systematically during core logging. In the holes examined in this study, approximately 60 percent of the copper in the logged drill holes was introduced during the late magmatic stage.

Type 2a veins are rare, wavy-edged quartz veins that contain minor chalcopyrite and bornite. They are the earliest formed veins in the felsic intrusions at Teniente (Table 3).

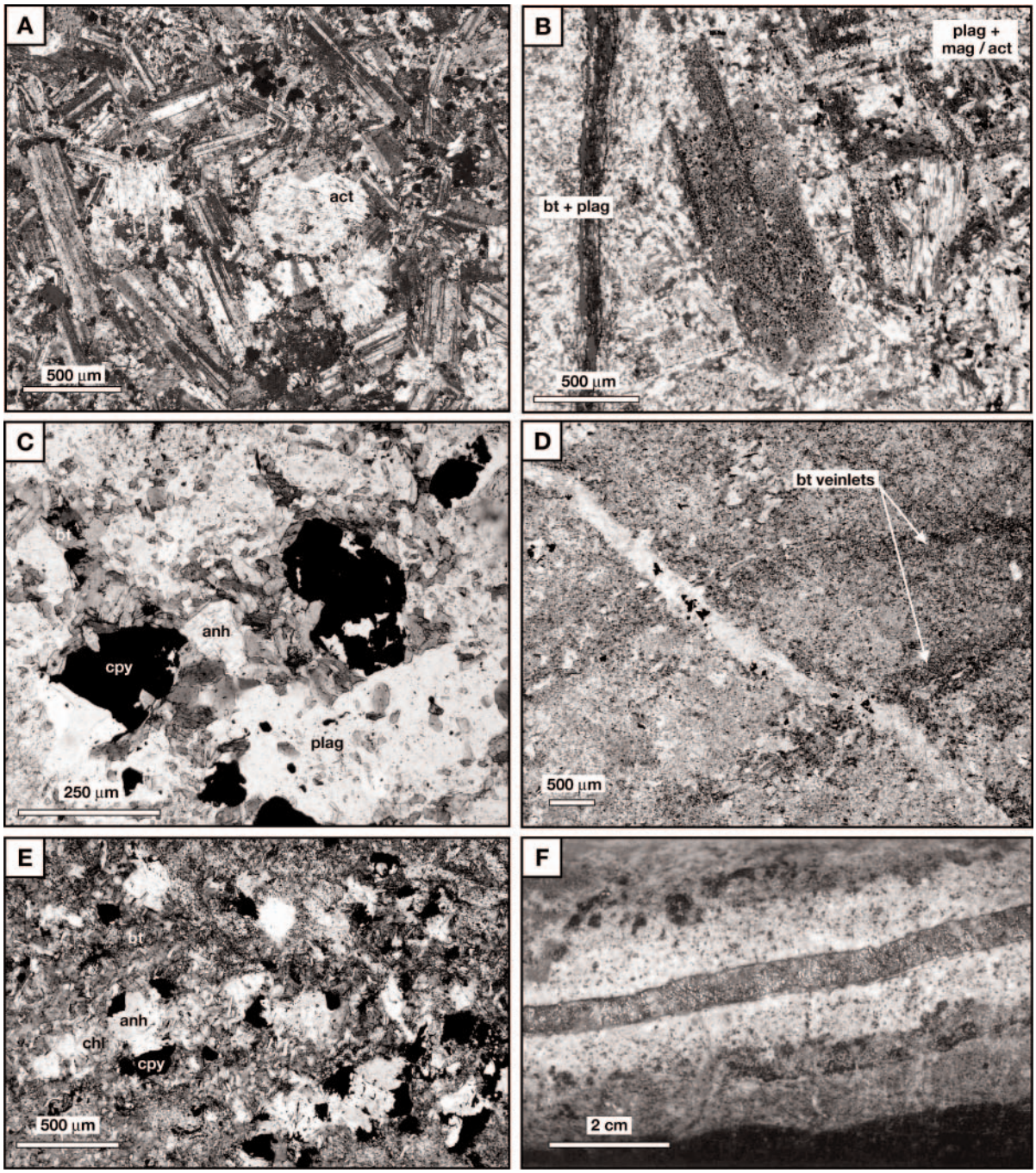

FIG. 7. Alteration styles at El Teniente. A. Fine andesite porphyry showing early magnetite alteration, which produced abundant secondary magnetite (typically 10–30 vol % of the rock) and variable amounts of actinolite. Note that primary igneous textures are preserved (ET604, DDH1565, 117.5 m, crossed polars). B. Late magmatic vein, on the left of the photo, with a biotite ± rutile halo that has preferentially altered the groundmass of early magnetite-altered mine andesite (right side of the dashed line). This is visible at the hand-sample scale in Figure 5B. Magnetite dusting in the plagioclase phenocryst is preserved (ET91, DDH1689, 236.4 m, plane-polarized light). C. Biotite-altered mine andesite. Aggregates of chalcopyrite, biotite, anhydrite, and rutile have replaced a primary mafic mineral (hornblende?; ET671, DDH1306, 208.3 m, plane-polarized light). D. Thin, diffuse brown biotite veinlets (+ minor anhydrite, chlorite, sulfides) and intense, texturally destructive biotite alteration that has overprinted the plagioclase phenocrysts and groundmass crystals. Groundmass magnetite has been altered to biotite ± rutile and sulfides. Biotite also occurs as a halo around the crosscutting late magmatic vein (ET664, DDH1306, 107.7 m, plane-polarized light). E. Pervasive alteration assemblage from the transitional potassic-propylitic zone (>300 m from dacite porphyry). Green-brown biotite is intergrown with clots of chlorite, sulfide (pyrite and chalcopyrite), and anhydrite (clear). Sericite needles and/or chlorite fans are intergrown with the disseminated and vein-hosted sulfides (ET62, DDH1738, 428.2 m plane-polarized light). F. Chalcopyrite + quartz + anhydrite principal hydrothermal vein with a phyllic halo. Note that the phyllic halo is zoned from inner sericite to outermost chlorite (ET44, DDH1738, 186.1 m). Abbreviations: act = actinolite, anh = anhydrite, bt = biotite, chl = chlorite, cpy = chalcopyrite, mag = magnetite, plag = plagioclase.

TABLE 5. Summary of Vein Paragenesis, Alteration, and Mineralization[1]

Vein type	Mineralogy	Features	Abundance Cu	Abundance Mo	Abundance VA	Associated intrusions, alteration, sulfides	
Premineralization stage							
1a veins	Magnetite, Ca plagioclase, quartz, actinolite, anhydrite	Thin, to several centimeters thick; diffuse veins with early magnetite alteration halo	-	-	R	Early magnetite alteration; related to Sewell Tonalite?	
1b veins	Quartz ± tourmaline, sericite, chlorite	Quartz veins (dikes) up to 8 m thick	-	-	R	Early phyllic alteration (sericite, chlorite, tourmaline); related to Sewell Tonalite?	
Late magmatic (LM) stage							
Anhydrite-sulfide-biotite breccias	Anhydrite breccias, veins + chalcopyrite (±biotite, tourmaline, feldspar)	Similar to type 2d anhydrite breccias, includes biotite or tourmaline; includes biotite-bearing vein types	A	C	R	**Early - gray porphyry**	Associated with potassic alteration (biotite, Na-K-feldspar), grading to distal propylitic alteration (chlorite, sericite, magnetite, epidote)
2a veins	Quartz ± chalcopyrite, bornite, anhydrite	Wispy, wavy-edged, thin, rare veins in dacite intrusions	C	-	R	**Main**	
2b veins	Chlorite, sulfide, anhydrite, quartz-biotite-Na-K-feldspar, anhydrite, quartz halo	Abundant, zoned veins, with Na-K-feldspar halos; 1 mm to 4 cm thick; temporal overlap with type 2c and 2d veins	C	R	A	**dacite porphyry dyke + pipes**	Type 2 distal (sericite-chlorite stable), and type 2 chlorite veins predominate in peripheral zones of deposit
2c veins	Quartz, anhydrite, sulfide (±K-feldspar, chlorite, biotite)	Abundant, submillimeter to 4 cm thick; ±biotite halo	C	R	A		
2d breccias	Anhydrite breccias (±sulfide)	Crackle breccia; associated with contacts of dacite intrusions; ±Na-K-feldspar or biotite halo	C	-	R		Contains bornite, chalcopyrite, molybdenite
2e veins	Quartz, sulfide (±anhydrite)	Thick (5 mm–3 cm), continuous, straight-edged; typical sulfide (+ molybdenite) seam and /or selvage; ±biotite or phyllic halo	C	C	C	**Late**	
2 chlorite veinlets	Sulfide, chlorite (±anhydrite, quartz, sericite, biotite)	Thin (<5 mm), abundant in propylitic zone; + chlorite, sericite halo; commonly form central seam in reopened veins (e.g., type 2b)	C	R	C		
Principal hydrothermal (PH) stage							
3 veins	Quartz, anhydrite, sulfide	Thick (up to 4cm) chalcopyrite-rich veins, minor gangue quartz and anhydrite; well developed sericite, chlorite, quartz halos	A	C	C	Phyllic halos + pervasive alteration; sulfides are chalcopyrite, pyrite, molybdenite (bornite absent); concentrated distally from dacite dike	
Late hydrothermal (LH) stage						Second phyllic (±illite) alteration stage, related to intrusion of Braden Breccia and latite dikes; veins are concentrated close to these intrusions	
4a breccias	Tourmaline, anhydrite, sulfide (±gypsum, quartz)	"Crackle breccia" and veins; pale sericite halo, tourmaline rimming walls; related to Marginal Breccia (?)	C	-	R		
4b veins	Anhydrite, chalcopyrite, bornite (±quartz, tourmaline, gypsum)	<2 cm thick; sericite ± chlorite halo; similar to type 3 veins, but they cut type 4a, and can contain bornite	C	R	R	Sulfides are chalcopyrite, bornite, pyrite, tennantite-tetrahedrite, molybdenite, (+ minor sphalerite, galena, enargite, stibnite); gangue minerals are anhydrite, quartz, tourmaline, gypsum, carbonate, barite	
4c veins	Carbonate (±various gangue and sulfides)	Sericite, chlorite halo; up to tens cm thick, variable vein mineralogies; include anhydrite breccias	C	A	C		
4d veinlets	Gypsum, chlorite (± various minerals)	Gypsum-chlorite dominated; typically hin, chlorite, tsericite halo; occur inside and outside the Braden Pipe.	-	-	R	Expostuma stage (Cuadra, 1986)	

[1] A relative scale of the estimated vein abundance (VA) and Cu and Mo Abundance for each vein stage is indicated: A = abundant, C = common, R = rare, - = absent

Unidirectional solidification textures (UST; Shannon et al., 1982; Kirkham and Sinclair, 1988; Fig. 8A), also containing copper sulfides, occur in some of the dacite pipes, and we infer a similar timing for the unidirectional solidification textures and the type 2a veins. They are both interpreted to have formed within a partly solidified igneous melt.

The oldest mineralized veins in the andesitic wall rocks are zoned, mineralogically complex type 2b veins with Na-K-feldspar halos (Fig. 8B-C, Table 3). The veins contain Cu-Fe sulfides, biotite, anhydrite, and quartz and typically show more than one stage of opening and sulfide precipitation (Fig. 8D). Type 2c veins are quartz-dominated veins (Fig. 8B), locally with biotite halos. They are more continuous than type 2a or 2b veins. Anhydrite ± copper sulfide-cemented crackle breccias (type 2d) formed within the mine andesites at the contacts with the dacites. Both type 2b veins and type 2d breccias cut and are cut by individual dacite intrusions, indicating multiple vein- and breccia-forming events overlapping in time with intrusion of the dacites. In general, type 2c veins cut type 2b veins (Fig. 8B) and the dacite contacts. Type 2b and 2c veins comprise the bulk of the late magmatic stockwork. Late-stage type 2e veins are up to 2 cm wide and typically contain molybdenite. They have parallel walls, inward-grown quartz crystals, central sulfide seams, and peripheral sulfide selvages (Fig. 8E).

There are some late magmatic vein types that are spatially restricted to specific parts of the deposit. Type 2 chlorite (intermediate argillic) veins are thin chlorite-sulfide–dominated veins that reopened earlier late magmatic stage veins locally. Biotite-(or tourmaline) anhydrite sulfide-bearing veins and breccias are concentrated adjacent to the gray porphyry in section 124. Type 2 distal veins are chlorite-sericite–bearing late magmatic veins that are concentrated at the margins of the deposit. These are interpreted to be temporally equivalent to the biotite-bearing type 2 veins in the core of the system. The mineralogy of some late magmatic veins varies with

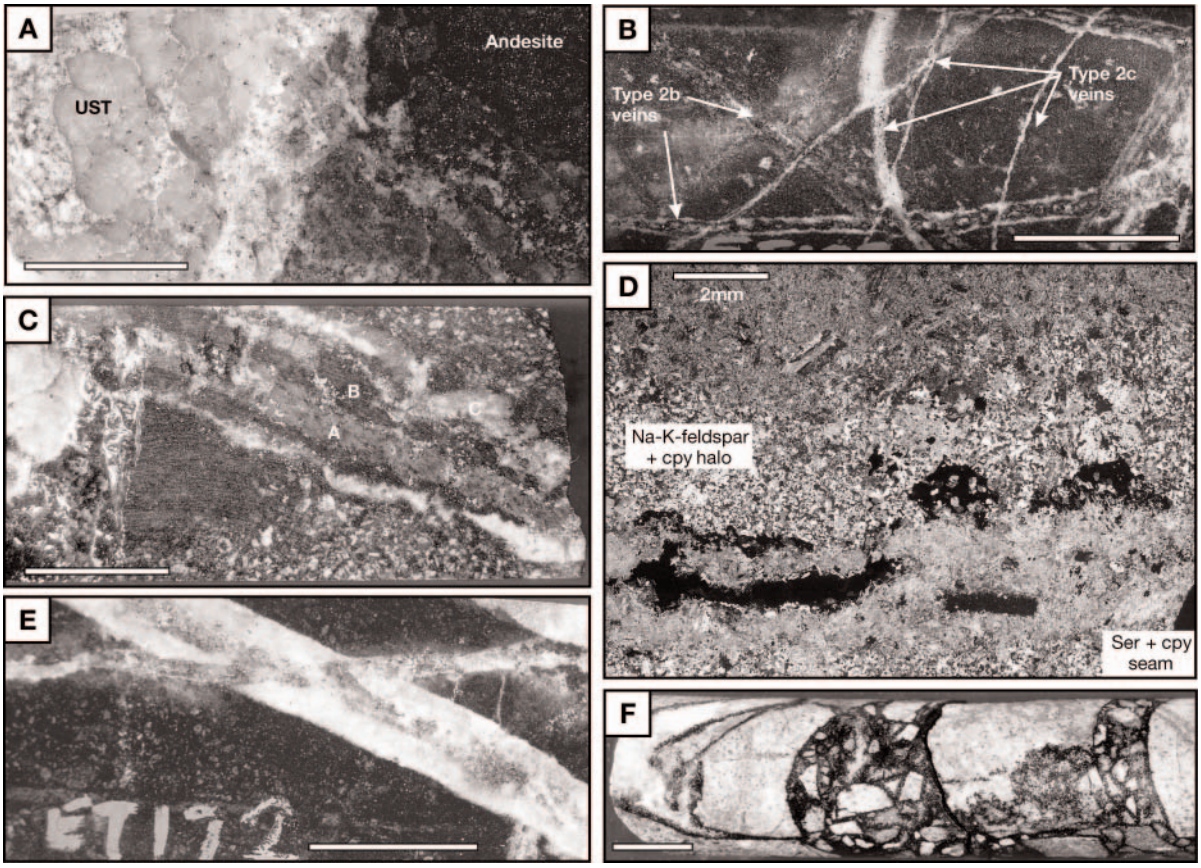

FIG. 8. Vein styles at El Teniente. A. Unidirectional solidification textures (UST) at the contact of a dacite pipe, with crystal orientations perpendicular to the intrusion walls. The dacite has cut a broad, diffuse type 2b vein in the mine andesites (ET697, DDH1889, 174.5 m). B. Wavy type 2b veins with pale Na-K-feldspar halos cut by straight type 2c quartz veins (ET102, DDH1689, 299.2 m). C. Andesite porphyry, cut by a thick type 2b chlorite + sericite + anhydrite + quartz vein (A), with a dark-gray biotite-rich selvage (B), and a pale-gray to white Na-K-feldspar halo (C; ET265, DDH1529, 233.6 m). D. Photomicrograph of a type 2b chalcopyrite-sericite vein with a halo of Na-K-feldspar, quartz, chalcopyrite (opaque, poikolitically enclosing quartz and feldspar), and anhydrite, which has overprinted biotite-altered andesite. Note the two generations of chalcopyrite and the partial replacement of early chalcopyrite + Na-K-feldspar by chalcopyrite + sericite (ET705, DDH1463, 61.3 m, crossed polars). E. Type 2e quartz vein, with straight sides, crystals perpendicular to the vein walls, and a central chalcopyrite seam, cut by a type 3 chalcopyrite-quartz with a thin phyllic halo (ET172, DDH1300, 165.6 m). F. Late hydrothermal type 4a tourmaline breccia composed of intergrown tourmaline and chalcopyrite around the vein walls, filled by anhydrite, and associated with phyllic alteration of the wall rock (ET520, DDH1418, 332.1 m). Abbreviations: cpy = chalcopyrite, ser = sericite, UST = unidirectional solidification texture (comb quartz layer).

depth. In the potassic alteration zone (see below), type 2b veins are predominant at depth, whereas type 2c veins are abundant at elevations above 2,000 m (Figs. 9A, 10A). At higher elevations, late magmatic veins also contain chlorite and sericite distal to the dacite intrusions (Fig. 10C).

Subvertical, polylithologic, matrix-supported biotite breccias (A. Skewes, unpub. report for CODELCO, 1997; Skewes et al., 2002) occur predominantly at the contacts between the felsic intrusions and andesitic wall rocks (Fig. 4). Rounded to subangular clasts of biotite-altered andesite and felsic intru-

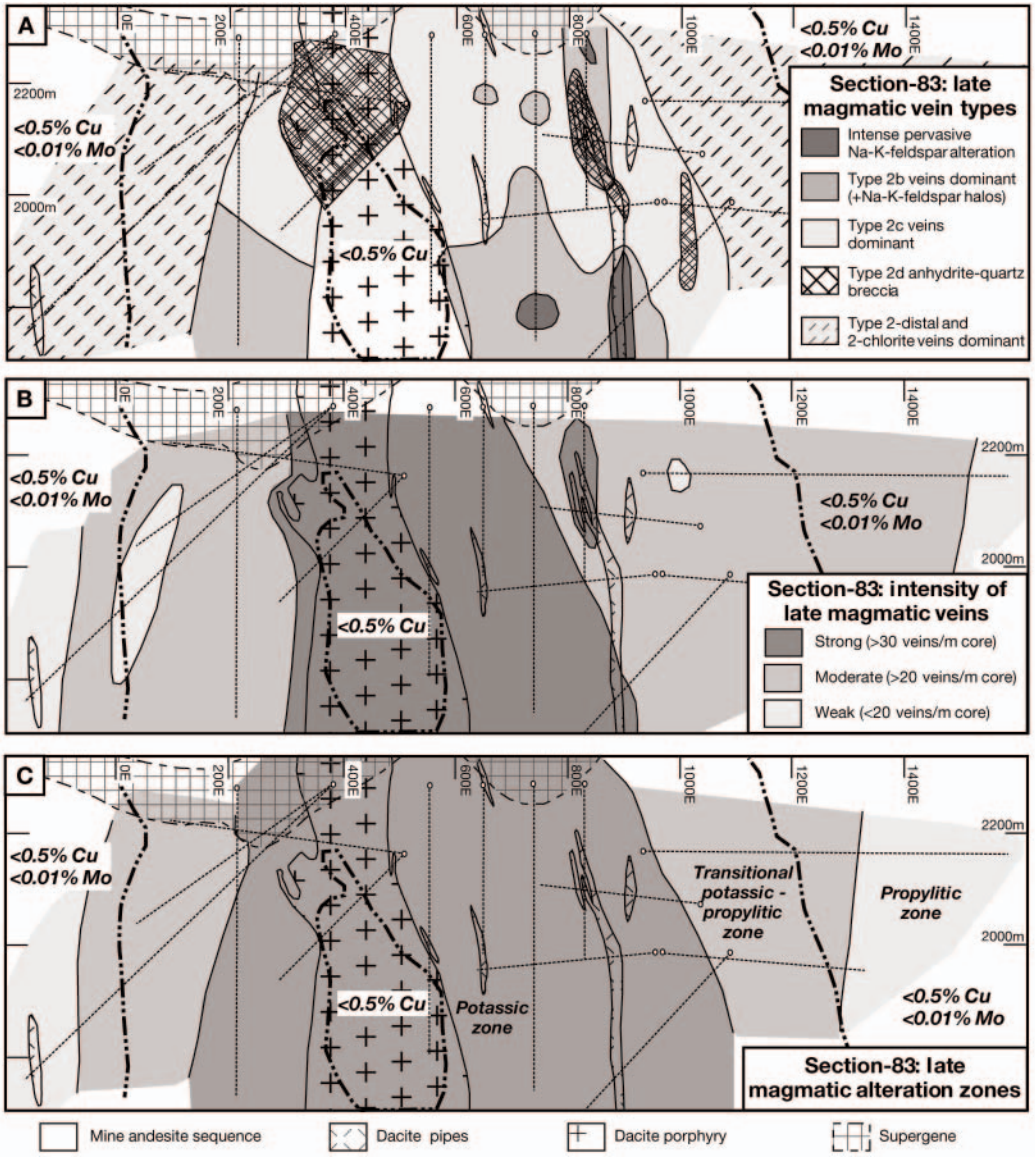

FIG. 9. A. Distribution of late magmatic vein styles in section 83. Type 2d anhydrite breccia zones are localized around the contacts of the dacite pipes and rarely the dacite porphyry. Type 2b veins are predominant at depth where they are associated with the vein-controlled and pervasive Na-K-feldspar alteration assemblage. Type 2c quartz veins are predominant at higher elevations. The thin vertical zone of anhydrite breccia at 1000E is presumably associated with a dacite pipe located off section to the south. Type 2 distal and chlorite veins are predominant at the periphery of the deposit. B. Abundance of late magmatic veins in section 83. High densities of late magmatic veins (up to 50 veins/m core) occur close to the dacite porphyry and locally around the dacite pipes. Late magmatic veins decrease in abundance away from the dacite porphyry, to intensities of 10 to 20 veins/m core in the propylitic zone. Note that it can be difficult to distinguish late magmatic and principal hydrothermal veins in the transitional potassic-propylitic zone due to the similarity in vein mineralogy, and reopening and alteration of late magmatic veins by later principal hydrothermal veins. C. Domains of late magmatic stage vein and/or alteration assemblages in section 83. The proximal potassic domain (see Table 6) occurs within 100 to 400 m of the dacite porphyry, in which the veins are biotite bearing and disseminated sulfides (bornite and chalcopyrite) are stable with respect to biotite (e.g., Fig. 7C). In the transitional potassic-propylitic zone, the late magmatic alteration and vein assemblages are sericite ± chlorite bearing (e.g., Fig. 7E). The outermost propylitic domain is marked by a decrease in vein and alteration intensity, an increase in the abundance of chlorite in the alteration assemblage, and pyrite (± minor pyrrhotite inclusions) to chalcopyrite ratios >5. Biotite grades from brown and Ti rich in the proximal potassic zone to green and Ti poor in the transitional and propylitic domains.

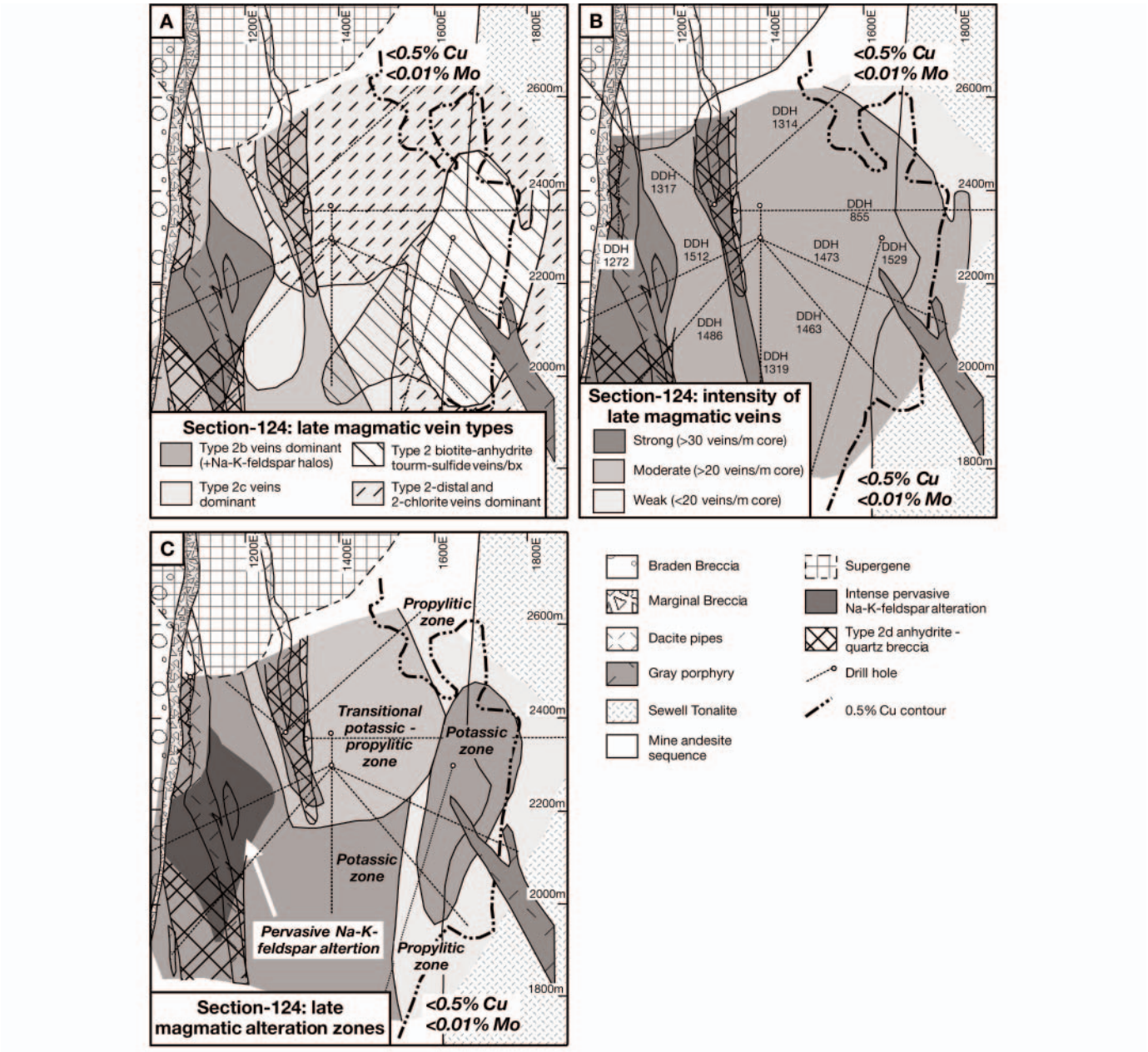

FIG. 10. A. Distribution of late magmatic vein styles in section 124. See (B) for drill hole numbers. This section contains an irregular zone of intense Na-K-feldspar alteration that has affected 100 percent of the rock volume localized around a dacite pipe. Around this Na-K-feldspar–altered zone are type 2d anhydrite breccias and domains of vein-controlled to pervasive Na-K-feldspar alteration. Type 2 distal and chlorite veins are abundant in the propylitic zone and at higher levels. Richly mineralized anhydrite-sulfide breccias occur adjacent to the gray porphyry. The breccias contain biotite below 2,100 m and tourmaline and sericite at higher levels. Note that the distribution of the geologic units in this section was obtained from the mine database, courtesy of CODELCO, and is based on more drill holes than indicated in (B). B. Abundance of late magmatic veins in section 124. High vein densities occur close to the dacite porphyry (west of the section) and locally around and downdip from the dacite pipes. Late magmatic veins are less abundant at the eastern edge of the section outside the 0.5 percent Cu ore shell boundary. C. Domains of late magmatic stage vein and/or alteration assemblages in section 124. The proximal potassic zone is localized around the dacite porphyry (to the west of the section) and includes zones of intense pervasive Na-K-feldspar alteration. The transitional potassic-propylitic zone occurs in the higher levels of the section. The propylitic domain occurs on the periphery of the deposit. Potassic-altered zones also occur around the gray porphyry where it has intruded the Sewell Tonalite and around the dacite pipe at 1300E. Abbreviations: bx = breccia, tourm = tourmaline.

sions (Fig. 5C) are set in dark-gray, hydrothermal cement composed of biotite, anhydrite, quartz, feldspar, Cu-Fe sulfides, molybdenite, and chlorite. The biotite breccias are locally difficult to distinguish from the altered mine andesites (e.g., Skewes et al., 2002). Most of the late magmatic, principal hydrothermal and late hydrothermal stage veins cut the

breccia bodies. There are, however, rare examples of (1) truncated quartz veins contained within some clasts, (2) discrete clasts of quartz veins, and (3) variable intensities of biotite alteration within adjacent clasts. These features are interpreted to indicate that formation of the biotite breccias postdated the earliest stages of late magmatic veining and alteration at El Teniente. One biotite breccia in section 83 (Fig. 4) cuts the dacite porphyry obliquely, and the common occurrence of felsic clasts in this breccia implies that it formed after the dacite. Our detailed logging shows that although the breccias contain significant amounts of disseminated copper and molybdenum sulfides, they only host a minor portion (<10%) of the ore in the logged drill holes at El Teniente.

Late magmatic vein types are systematically zoned around the dacite intrusions, and their development varies with depth (Figs. 9A, 10A). The intensity of late magmatic veins is highest within 300 m of the dacite porphyry and locally around the dacite pipes (Figs. 9B, 10B). Based principally on the vein and alteration mineral assemblages, three late magmatic domains can be distinguished: (1) proximal potassic zone (biotite bearing), (2) transitional potassic-propylitic zone (biotite-sericite-chlorite bearing), and (3) propylitic zone (chlorite bearing, Figs. 9C, 10C). The features of these zones are summarized in Table 6.

Within the dacite intrusions, potassic (-sodic) alteration associated with the late magmatic stage is characterized by hydrothermal K-(±Na-) feldspars. The feldspars are white in hand specimen, and staining or thin section petrography is required to discriminate orthoclase and albite. Primary biotite is partially to completely altered to chlorite ± carbonate. Phenocryst and groundmass plagioclase show weak to strong selective alteration to sericite ± carbonate. The K-(±Na) feldspar alteration assemblage is developed pervasively at the southern end of the dacite porphyry and is restricted to vein halos in the northern sector (Ossandón, 1974; Camus, 1975). At the northern end of the dacite porphyry, the K-(±Na) feldspar alteration assemblage passes laterally northward to a propylitic assemblage of chlorite, epidote ± magnetite, hematite, pyrite, sericite, and calcite (Ossandón, 1974).

Domains of intense, pervasive domains of Na-K-feldspar alteration occur in the andesites adjacent to some of the dacite pipes, extending up to 50 m away, and, to a lesser degree, the dacite porphyry. The Na-K-feldspar–altered zones are composed of massive anhedral gray quartz and sodic feldspar ($Ab_{44–96}$, predominantly $Ab_{61–96}$), and lesser anhydrite, rutile, sulfides, and minor biotite. Minor pervasive alkali feldspar ($Or_{13–96}$) was detected, and staining indicates the existence of variable amounts of K-feldspar in the assemblage.

Apart from these localized zones, potassium metasomatism in the andesites has caused intense, texturally destructive, pervasive biotite alteration of the groundmass and mafic phenocrysts, in many cases leaving the plagioclase phenocrysts unaltered (Fig. 7B). The biotite-altered zone is laterally extensive, extending up to 1 km away from the dacites. Intensely biotite altered andesites are composed only of dark-brown biotite, rutile, anhydrite, and Cu-Fe sulfides (Fig. 7C-D). Early, microscopic biotite veinlets (Skewes et al., 2002; Fig. 7D) and late magmatic stage veins with biotite halos are abundant locally (Fig. 7B).

With increasing distance from the dacite porphyry (typically >300 m), hydrothermal chlorite and sericite occur together with hydrothermal biotite. The abundance of these phases increases outward toward the propylitic alteration zone, whereas biotite abundance decreases outward (Fig. 7E). Biotite in the transitional alteration zone has a distinctive green-brown color typical of low titanium biotite when viewed in plane-polarized light (electron microprobe analyses indicate <0.25 wt % Ti; Cannell, 2004). Low Ti biotite

TABLE 6. Characteristics of the Potassic, Transitional Potassic-Propylitic and Propylitic Alteration Zones at El Teniente

	Potassic zone	Transitional potassic-propylitic zone	Propylitic zone
Location	Proximal to dacite porphyry and locally around dacite pipes	Distal from dacite porphyry, and >2,200-m elevation	Deposit periphery, near and extends beyond the 0.5 percent Cu limit
Dominant pervasive alteration assemblage	Biotite alteration assemblage	Transitional potassic-propylitic assemblage	Propylitic assemblage
Other alteration types	Pervasive Na-K-feldspar alteration	Pervasive phyllic alteration, vein controlled Na-K-feldspar alteration	Rare phyllic (phengitic sericite), early magnetite ± epidote
Dominant vein/breccia type	Type 2a-2e, type 2 biotite-anhydrite-sulfide breccias, biotite breccias	Type 2 distal, type 2f chlorite, type 3	Type 2f chlorite, type 2 distal
Vein intensity	High	Medium-high	Low
Vein gangue mineralogy (ubiquitous quartz, anhydrite)	Biotite, Na-K-feldspar, rare sericite, chlorite.	Sericite, chlorite, rare Na-K-feldspar, magnetite	Chlorite, pyrite ±sericite, magnetite, Na-K-feldspar
Sulfides	Chalcopyrite and bornite	Chalcopyrite and pyrite	Pyrite ± chalcopyrite pyrrhotite inclusions
Phyllosilicate mineral intergrown with sulfides	Biotite	Sericite and chlorite	Chlorite ± sericite
Cu and Mo grades	High Cu (>1%) and Mo (>0.01%)	High-moderate Cu (mostly >1%), moderate Mo (mostly 0.01–0.03%)	Low Cu (<0.5%), and Mo (<0.01%)

compositions are consistent with a lower temperature of formation (Engel and Engel, 1960; Le Bel, 1979). Pyrite (±pyrrhotite inclusions) and magnetite are abundant in the transitional zone, whereas bornite is absent. Chlorite ± sericite typically occur as rims around sulfide grains (Fig. 7E).

The transitional alteration assemblage grades out to a propylitic alteration assemblage within the andesitic country rocks, outboard from the 0.5 percent Cu contour. Mafic minerals are selectively altered to chlorite, magnetite, epidote, and hematite. This assemblage also has filled amygdales in the propylitic zone (Villalobos, 1975).

The dacite intrusions have an intimate spatial association with the pervasive alteration assemblage, with the vein intensity, and with the vein styles (Figs. 9, 10). In particular, intense pervasive Na-K-feldspar alteration and abundant type 2b veins and 2d breccias (up to 30% of the rock volume) occur at the contacts of some of the dacite pipes resulting in high copper (±Mo) grades localized around the pipe contacts. Although the dacite porphyry dike typically does not display such an obvious relationship to mineralization, the large-scale zoning of alteration assemblages, vein intensity, vein styles, and sulfide mineralogy around the southern end of the dike, and the temporal overlap between veining and intrusion suggest that alteration and mineralization are genetically associated with the dike.

Principal hydrothermal stage (type 3 veins)

Late magmatic stage veins are overprinted by principal hydrothermal stage veins and associated phyllic alteration halos. Principal hydrothermal (type 3) veins are typically thick (2 mm–3 cm) and chalcopyrite-rich (±molybdenite, ± pyrite at the periphery of the deposit). They have well-developed phyllic alteration halos from 3 mm to 5 cm thick (Fig. 7F). Quartz and anhydrite are the predominant gangue minerals. Although principal hydrothermal veins have lower abundances (typically <10 veins/m of core) than the late magmatic veins, our visual estimate is that principal hydrothermal veins host approximately 30 percent of the copper in the logged core.

In addition to alteration halos around principal hydrothermal veins, intense, texturally destructive phyllic alteration occurs in discrete domains in the higher levels of the mine at Teniente. These intensely phyllic altered intervals are composed of sericite (up to 80%), quartz (5–25%), variable chlorite (0–15%), and minor anhydrite, rutile, and sulfides (up to 5%). Infrared absorption analysis using a portable infrared spectrometer (PIMA) indicates that the white mica from the principal hydrothermal stage varies of the principal hydrothermal stage varies from slightly paragonitic to slightly phengitic muscovite.

Estimated densities of principal hydrothermal veins and intensities of alteration are shown for sections 83 and 124 in Figures 11 and 12, respectively. Intensity of phyllic alteration and densities of principal hydrothermal veins are highest in the upper levels of the deposit, where they overprint the transitional potassic-propylitic zone. In these domains, pervasive phyllic alteration affected up to 100 percent of the rock volume locally (Zúñiga, 1982; Figs. 11B, 12B). The intensity of phyllic alteration and the density of principal hydrothermal veins decrease with increasing depth and with increasing proximity to the dacite porphyry. Below 2,150 m, phyllic alteration only occurs as centimeter-scale halos around type 3 veins, except on the west side of section 83 (Fig. 11).

Late hydrothermal stage (type 4 veins)

The late hydrothermal stage is a second phyllic stage spatially and temporally associated with the Braden Pipe and related latite intrusions. Of all of the vein types, only late hydrothermal veins cut the Braden Pipe, providing temporal constraints on the formation of the final stage of the vein paragenesis.

Late hydrothermal veins have a diverse mineralogy, including Cu-Fe, Mo, and base metal sulfides and sulfosalts (Table 5). Gangue minerals include quartz, anhydrite, tourmaline, gypsum, carbonates, and barite. Clay minerals and pyrophyllite were also reported from this stage (Camus, 1975). PIMA analyses (Cannell, 2004) indicate that sericite of the late hydrothermal stage is more illitic than that of the principal hydrothermal stage. Kaolinite was detected in only one of more than 50 samples analyzed.

Type 4a veins and crackle breccias contain tourmaline, anhydrite, and chalcopyrite (Fig. 8F, Table 5) and are interpreted to be associated with the Marginal Breccia facies of the Braden Pipe. They are cut by type 4b quartz-chalcopyrite-anhydrite (±bornite) veins that are mineralogically and texturally similar to type 3 veins. Type 4c veins are mineralogically variable, typically containing carbonates, sulfates, sulfides (including abundant molybdenite), and sulfosalts (Table 5). Type 4c veins occur in some of the larger faults observed underground. Type 4b and 4c veins are less abundant in the Braden Pipe than in the adjacent mine andesites. Spectacular crystal caverns containing gypsum crystals up to 6 m long occur within the Braden Pipe. These are attributed to stage 4c hydrothermal activity. The youngest veins are thin, typically unmineralized type 4d gypsum-chlorite veins.

Late hydrothermal veins are less abundant than principal hydrothermal veins, and we estimate that they host approximately 10 percent of the copper in the logged drill holes. The density of late hydrothermal veins and the intensity of alteration are greatest within 100 to 200 m of the Braden Pipe and decrease away from the pipe and with depth. South of the Braden Pipe, thin latite dikes are locally associated with richly mineralized type 4c breccia zones and domains of pervasive phyllic alteration.

Structural Evolution

A diversity of vein arrays has been documented in porphyry deposits. Stockwork orientations can be described as random (e.g., "A" veins from El Salvador: Gustafson and Hunt, 1975) or sheeted, in which one or more preferred orientations exist (Laramide deposits of Arizona: Heidrick and Titley, 1982; Titley, 1990; Cadia Hill; Holliday et al., 2002). A sheeted vein system indicates that far-field stresses exceeded the stresses localized by magma emplacement and, as a consequence, the veins are predominantly orientated parallel to the regional fabric (Titley, 1990; Tosdal and Richards, 2001). Some deposits show domains of preferred vein orientation that formed in response to displacement along master faults (e.g., Chuquicamata: Lindsay et al., 1995). Concentric and radial vein and dike patterns in several porphyry Cu and Mo deposits from the American Southwest (Titley, 1990; Tosdal and Richards, 2001), from "D" veins at El Salvador (Gustafson

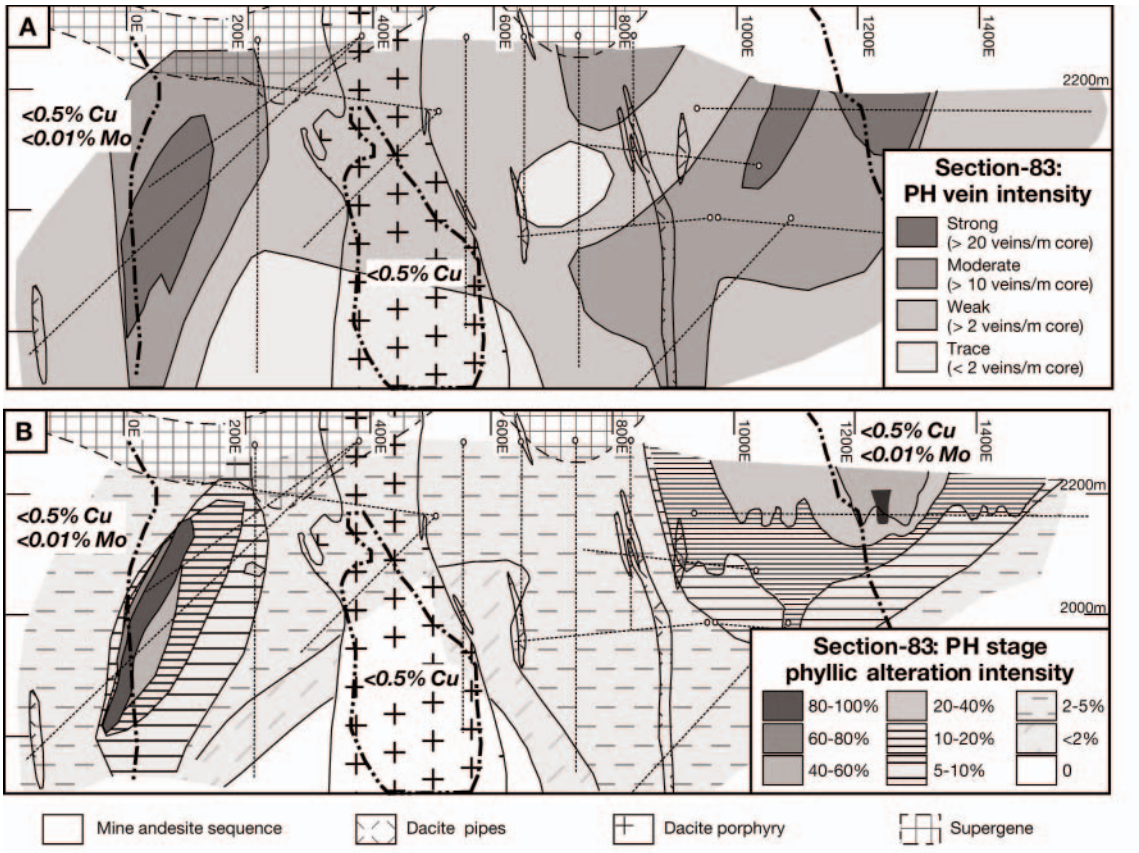

FIG. 11. A. Abundance of type 3 (principal hydrothermal) veins in section 83. Type 3 veins are only weakly developed near the dacite porphyry, especially at depth. Principal hydrothermal veins are more abundant away from the dacite porphyry and vertically upward, reaching a maximum of >20 veins/m core in the transitional zone. B. Intensity of phyllic alteration in section 83, which approximately correlates with abundance of principal hydrothermal veins. Intensity of phyllic alteration increases away from the dacite porphyry and also increases vertically, forming zones of pervasive alteration (solid colors) above 2,100 m RL. Below this level the phyllic alteration assemblage occurs as vein halos (lines and dashes). Chalcopyrite-rich type 3 veins do not have phyllic halos where they occur adjacent to the dacite porphyry at depth. Abbreviation: PH = principal hydrothermal.

and Hunt, 1975), and from various epithermal deposits (Rytuba, 1994, and references therein) have been described.

El Teniente was previously described as structurally isotropic, composed of a stockwork of randomly oriented veins, with the exception of a zone extending for ~200 to 300 m around the Braden Pipe that is composed of radial and concentric veins centered on the pipe (e.g., Cuadra, 1986). Subvertical strike slip and reverse faults occur in the deposit with a late hydrothermal vein fill, but these faults only have meter-scale displacements and can be traced for a maximum of 800 m (Cuadra, 1986; I. Garrido, 1995, unpub. report for CODELCO). There is a preferred northeast orientation for some faults, tourmaline-anhydrite breccia zones, latite, and lamprophyre dikes, and thick quartz veins (type 1b). Based on this preferred orientation of geologic features, the northeast Teniente fault zone (Fig. 2) has been implicated in the genesis of the deposit (Garrido et al., 1994). The north-northwest–trending dacite porphyry dike and the northwest-trending dacite pipes and associated igneous and anhydrite breccias to the northeast of the Braden Pipe (Skewes et al., 2002) are subparallel to the Codegua fault (Fig. 2).

A review of the available structural data from El Teniente was undertaken to ascertain the dominant vein and fault orientations and to relate them to the observed paragenesis, intrusive history, and district-scale structures. Vein and fault data were compiled from geotechnical reports and structural maps. No new measurements were collected for this study, and the data are paragenetically constrained to the late magmatic, principal hydrothermal or late hydrothermal stages as mapped by El Teniente mine geologists. In total, 4337 vein and fault measurements were utilized in this study from four mining areas (Quebrada Teniente, Sub-6, Esmerelda, and Regimiento). Where possible, the data are split into a late hydrothermal domain (where late hydrothermal veins predominate over principal hydrothermal veins) within approximately 200 to 300 m of the Braden Pipe and a principal hydrothermal domain (where late hydrothermal veins are rare) located outboard of the late hydrothermal domain.

Vein stages

The preferred structural orientations for the Teniente paragenetic stages are summarized in Table 7. Data for late

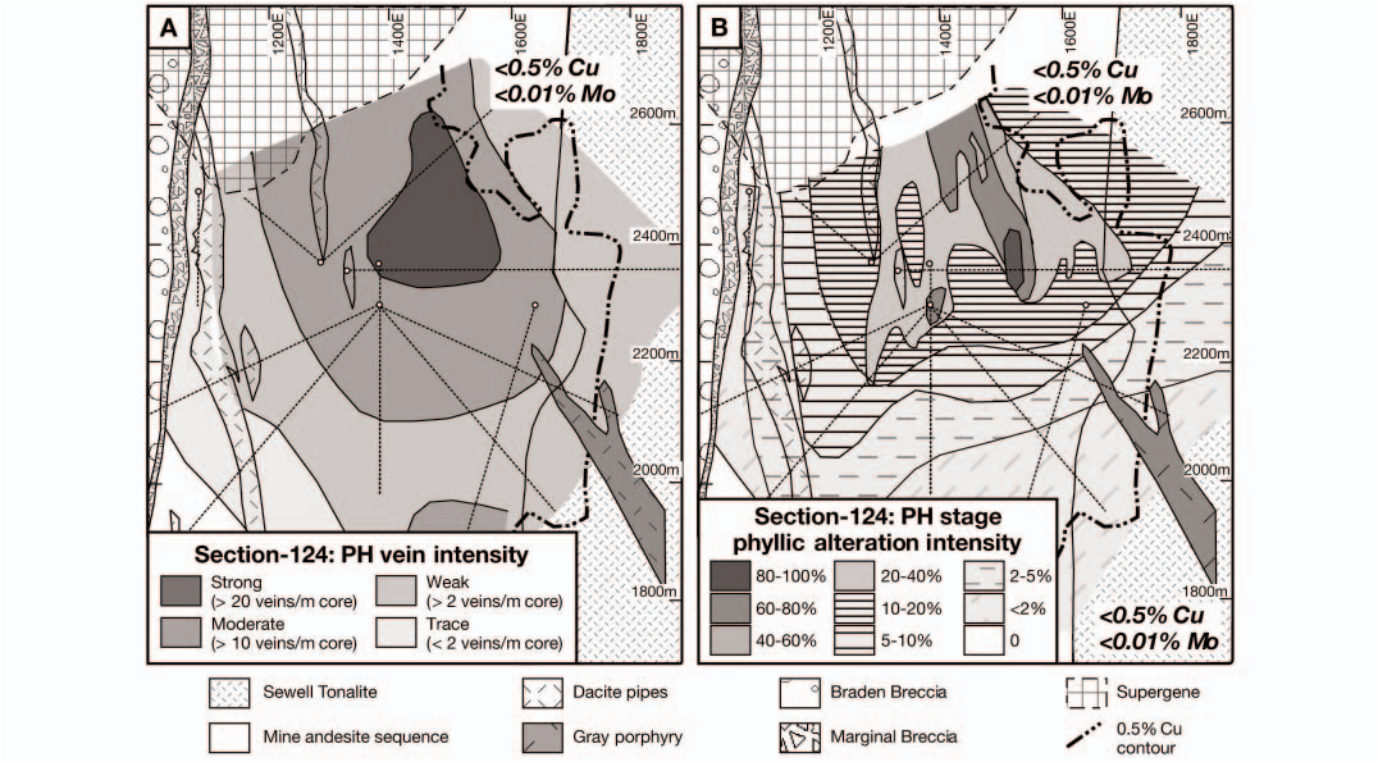

FIG. 12. A. Abundance of type 3 (principal hydrothermal) veins in section 124. Type 3 veins are most abundant in the transitional zone of section 124. Type 3 veins do not occur at depth to the west of the section, proximal to the Braden Pipe. B. Intensity of phyllic alteration in section 124. Pervasive phyllic alteration is restricted to levels above 2,200 m, within the transitional zone. Abbreviation: PH = principal hydrothermal.

magmatic and principal hydrothermal veins are plotted in stereonets in Figure 13A and B, respectively. Figure 13C and D plot the same structures in polar coordinates, relative to the radial angle from the geographic center of the deposit. In polar coordinates, a radial vein anywhere in the deposit has a north-south strike; a concentric inward-dipping vein anywhere in the deposit will have an east-west strike and a dip to the south.

TABLE 7. Summary of Vein Types at El Teniente (based on analyses of vein orientations and timing relationships)

Vein type	Orientations	Comments
Type 1b	Variable in mine, northeast in district	Premineralization, associated with Sewell Tonalite?
Type 2 (LM) and 3 (PH)	Concentric dipping (40°–80°) and radial (subvertical), broad data scatter	Associated with dacites; Type 2 veins are scattered, Type 3 veins are more focused
Type 4a-c (LH)	Concentric, typically >70°	Reverse faults common, associated with Braden Pipe
Type 4c, d (LH)	Northeast trending, subvertical	Mainly faults (strike slip), lesser veins, parallel to the Teniente fault zone
Type 4 (LH)	N ± 30°	LH veins that do not fit into sets 3 or 4

Abbreviations; LH = late hydrothermal, LM = late magmatic, PH = principal hydrothermal

Thick type 1b quartz veins have predominantly northeast trends, parallel to the Teniente fault zone. Northwest- and east-trending veins are also present (Fig. 14). The late magmatic and principal hydrothermal vein stockworks, which contain most of the copper in the deposit, have broadly concentric and radial orientations centered approximately in the middle of the deposit, where the Braden Pipe is now situated (Fig. 14). The concentric veins are shallowly dipping (predominantly 40°–60°) toward the pipe in the mine areas to the north of the Braden Pipe. They dip steeply (>60°) toward the Braden Pipe in the eastern sector and less steeply in the south of the deposit. Radial veins are subvertical and are more abundant in the principal hydrothermal domain than in the late hydrothermal domain. In all of the mine areas, shallowly dipping (<40°) vein populations are present. The preferred alignment of the late magmatic and principal hydrothermal veins in subvertical radial and inward-dipping concentric orientations with respect to the center of the deposit is shown in Figure 13C and D.

Most of the late hydrothermal structures have a consistent steeply inward dipping (>70°) concentric orientation with respect to the Braden Pipe (Fig. 15), illustrated in the stereonet data (Fig. 13F). fault orientations in the deposit (Figs. 13H, 16) have a similar orientation. In contrast to late magmatic and principal hydrothermal veins, radial and shallow-dipping concentric veins and faults are rare.

A series of planar northeast- to east-northeast–trending, subvertical late hydrothermal structures (Figs. 14G, 16) are

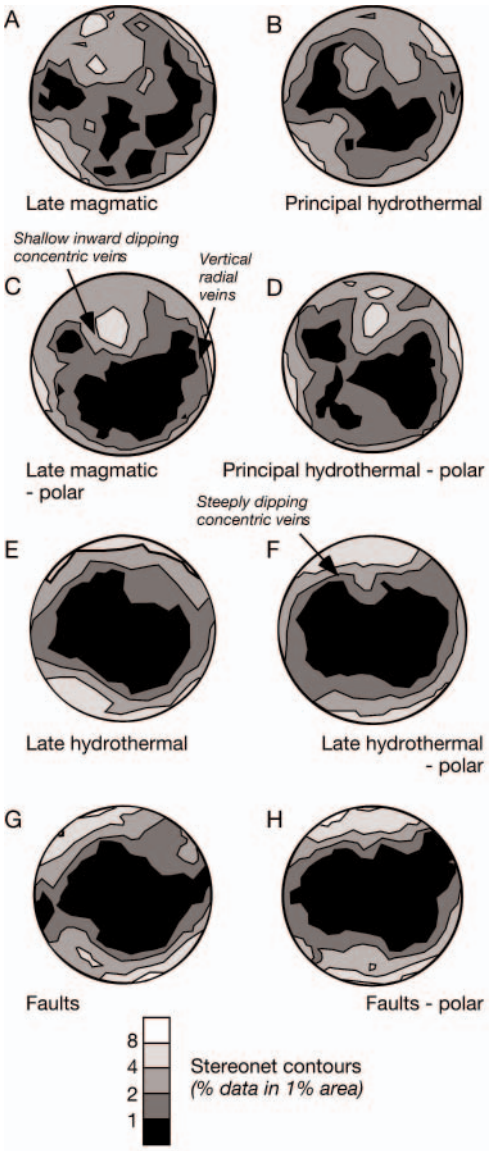

FIG. 13. Contoured stereonets showing poles to vein and fault orientations for El Teniente. Contour intervals are % data/1% area. A and B. Late magmatic (n = 463) and principal hydrothermal (n = 1,176) veins, respectively. Note the broad scatter of data for both datasets. C and D. Late magmatic (n = 463) and principal hydrothermal (n = 1,176) veins, respectively, plotted in polar coordinates, relative to the radial angle from the geographic center of the deposit. The radial angles assigned to the mine areas are Quebrada Teniente +25°, Sub-6 mine –20°, Esmerelda late hydrothermal domain –35°, Esmerelda principal hydrothermal domain –50°, Regimiento –200°. Note the concentration of shallow to steep inward dipping concentric veins and subvertical radial veins for both polar datasets. E. Late hydrothermal veins (n = 1,272), with consistently, steep dips, and variable strike. F. Late hydrothermal veins (n = 1,272) plotted in polar coordinates. Note the tight cluster of steeply inward dipping orientations concentric to the Braden Pipe. G. faults (n = 1,602), which have a consistently steep dip. The set of northeast-trending faults is visible in this dataset. H. faults (n = 1,602) plotted in polar coordinates. Despite the presence of northeast-trending faults, the faults are predominantly steeply inward dipping and concentric to the Braden Pipe. Structural information was compiled for this study from unpublished CODELCO geotechnical reports on individual mine areas by A. Morales and J. Pereira (1996), A. Morales and J. Seguel (1998), O. Quezada (1998), A. Russo (1999), A. Brzovic (1999, 2000), and Duarte (2000). The structural data were collected by the mine geologists during routine structural mapping or from strategically selected lines of detail, where all the structures are measured that cross a horizontal line on the wall of a drive. All data provided courtesy of CODELCO, El Teniente division.

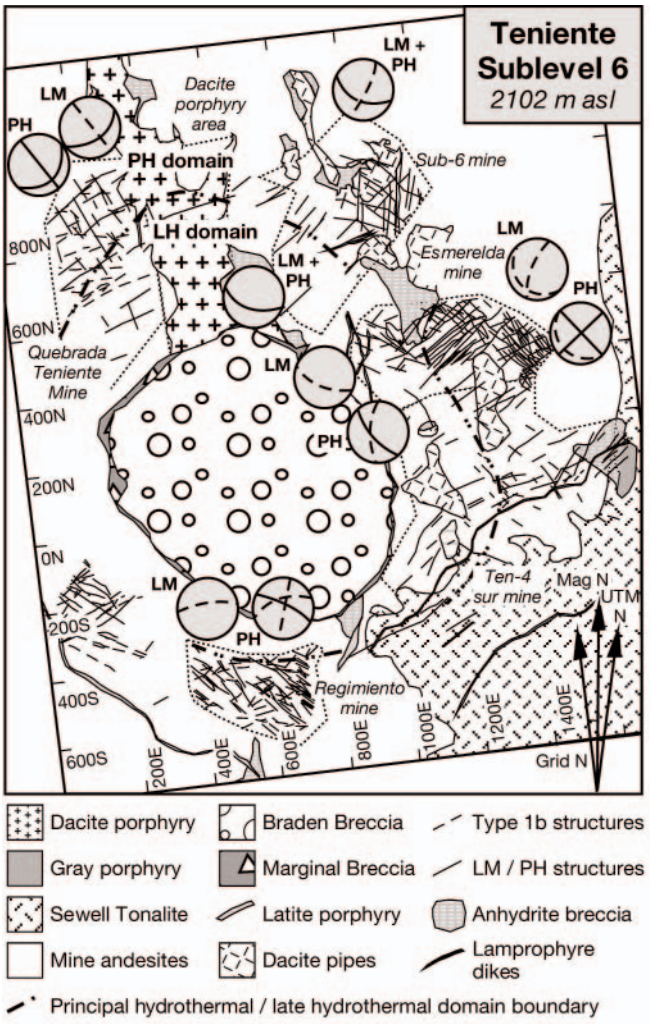

FIG. 14. Orientations of major (i.e., >50 m long) type 1b premineralization quartz veins and late magmatic (LM) and principal hydrothermal (PH) structures. Data for this figure, and for Figures 16 and 17, were obtained from 1:1000 and 1:5000 mapping by Teniente mine geologists (listed in Fig. 13). Stereonets indicate the dominant orientations (solid lines) and subdominant orientations (dashed lines) of veins measured by mine geologists during structural mapping. The dominant preferred orientation in the stereonets for the late magmatic and principal hydrothermal veins is approximately concentric to the Braden Pipe in all but the stereonet for late magmatic veins from Regimiento. Similarly, the major structures have mostly concentric and radial orientations. The dotted line concentric to the Braden Pipe is the approximate boundary between the late hydrothermal (LH) domain (within approx 300 m of the pipe) and the principal hydrothermal (PH) domain, which occurs farther out from the pipe. The rotated grid indicates the mine coordinates relative to magnetic and UTM north. Block-cave mining areas (e.g., Sub-6 mine) are denoted by dotted lines and contain most of the mapped structural features shown here. Abbreviations: asl = above sea level, LH = late hydrothermal, LM = late magmatic, PH = principal hydrothermal.

parallel to the Teniente fault zone (Fig. 2). Northeast-trending structures are mainly latest stage faults and include the "falla P," "falla D2," and the "falla ten-sur" anastomosing fault systems, the most continuous in the deposit (Cuadra, 1986). Some late magmatic and principal hydrothermal veins also occur in this orientation, implying that it was weakly developed during the main stages of veining and mineralization.

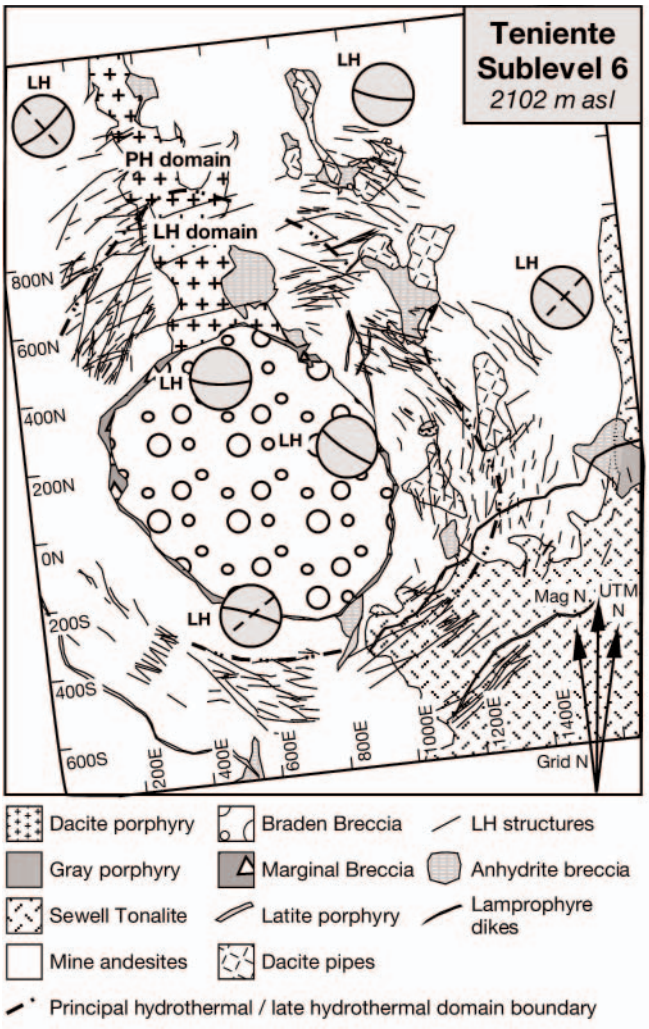

FIG. 15. Orientations of late hydrothermal major concentric structures and stereonets showing the orientations of late hydrothermal veins. See Figure 14 for detailed explanation. All of the stereonets of late hydrothermal veins indicate a predominant orientation concentric and steeply inward dipping to the Braden Pipe. Abbreviations: asl = above sea level, LH = late hydrothermal, LM = late magmatic, PH = principal hydrothermal.

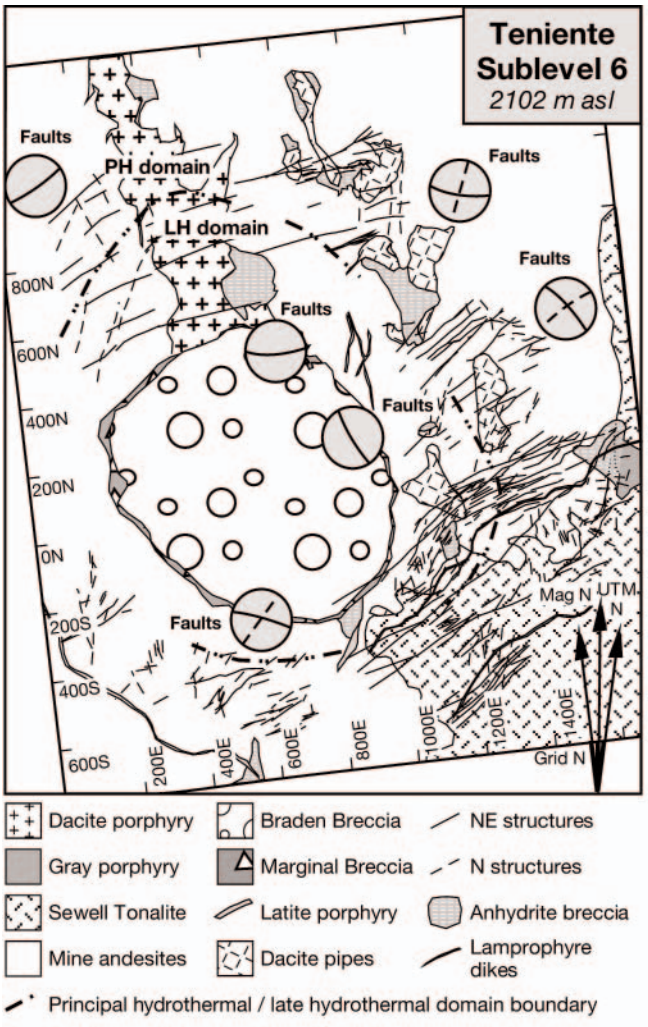

FIG. 16. Orientations of northeast-trending major structures, which are parallel to the district-scale Teniente fault zone. See Figure 14 for detailed explanation. Most of the northeast-trending structures formed during and after the late hydrothermal stage; however, the anisotropic zone adjacent to the Sewell Tonalite includes some late magmatic and principal hydrothermal veins. The stereonets plot all the faults in the deposit, predominantly with orientations concentric to the pipe. Some of the stereonets (Regimiento, Esmerelda) show a weak northeast-trending (or radial) secondary orientation. Other structures are predominantly north trending (±30°) and do not fit with the above sets. Abbreviations: asl = above sea level, LH = late hydrothermal, PH = principal hydrothermal.

Another minor set of late hydrothermal structures is predominantly north trending (Table 7, Fig. 16).

There is a pronounced structural anisotropy where structural sets coincide. For example, in the Quebrada Teniente mine area, concentric late hydrothermal structures occur parallel to the east-northeast–trending structures. In the Regimiento, Sub-6, and Esmerelda mine areas these structures are oriented obliquely to each other, resulting in a scattered vein and fault array.

Structural model

We propose a structural model based on the observed orientations and paragenesis of the veins and faults. Previous authors (e.g., Garrido, 1994) inferred that the northeast-trending Teniente fault zone was active during the period of formation of the late magmatic and principal hydrothermal stockwork. However, the vein stockwork at El Teniente does not have a sheeted orientation, suggesting that during vein formation, far-field stresses were less important than localized stresses around the felsic intrusive body. The late magmatic and principal hydrothermal vein orientations have an overall inward-dipping concentric and radial distribution centered in the middle of the deposit, coincident with the location of the Braden Pipe (Fig. 17A), suggesting that they formed in response to intrusion of a large pluton at depth and doming of the overlying volcano-sedimentary sequence (e.g., Acocella et al., 2000). The scatter of vein orientations may be due to local fluid pressures exceeding stresses induced by the intruding magma (e.g., Burnham, 1979). During the late magmatic stage, the dacite porphyry dike and pipes intruded

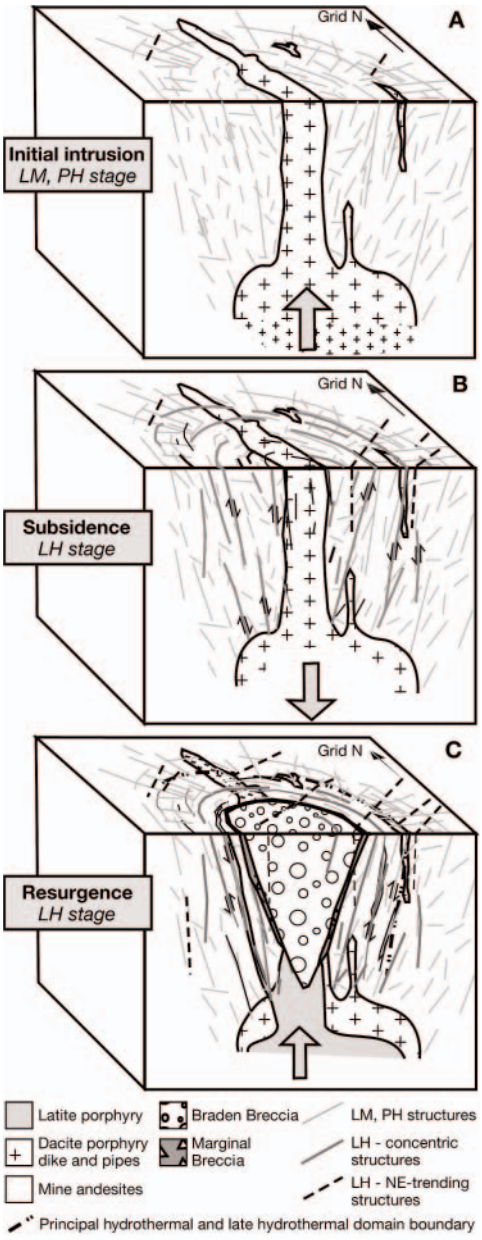

FIG. 17. Schematic structural model of El Teniente system. A. The vein stockwork emplaced during the late magmatic and principal hydrothermal stages was subjected to stresses associated with initial intrusion of a large pluton inferred to lie below the current level of the mine. Radial veins are more abundant peripherally (in the principal hydrothermal domains). Faults are rarely preserved from the late magmatic stage, probably due to reactivation and overprinting during the principal hydrothermal and late hydrothermal stages. B. A period of magmatic quiescence and subsidence followed, accompanied by magma withdrawal, in which steeply dipping normal concentric fractures were developed. C. A stage of resurgence of the magma chamber is inferred, and uplift was facilitated by reactivation of the concentric fractures with a reverse sense. Latite dikes, pebble dikes, Marginal Breccia zones, and late hydrothermal veins were emplaced into these extensional concentric fractures, until explosive brecciation and formation of the Braden Pipe caused instantaneous depressurization and cooling of the magma. Only minor alteration and veining followed this event, largely confined to concentric fractures inside and at the edges of the pipe overprinting the Marginal Breccia-Braden Breccia contact (R. Floody, 2000, unpub. report for CODELCO) and northeast-trending fractures related to movements along the Teniente fault zone. Abbreviations: LH = late hydrothermal, LM = late magmatic, PH = principal hydrothermal.

from the deep magma chamber into the mine andesites, and perturbations in the stress field caused by these high-level intrusions resulted in greater vein densities proximal to their margins (Figs. 9B, 10B).

A change in stress conditions led to the generation of concentric, subvertical fractures above the magma chamber during the late hydrothermal stage. The lack of radial veins in this stage implies that magma pressure was low, and it is interpreted that structures associated with the late hydrothermal stage formed during a subsidence event associated with magma withdrawal (e.g., Koide and Bhattacharji, 1975; Fig. 17B). Previously formed, steeply inward dipping reverse and outward dipping normal concentric faults would have been reactivated with opposite sense, allowing for central subsidence (Acocella et al., 2000).

In this model, resurgence occurred in the deep magma chamber during the late hydrothermal stage, associated with uplift, fracture reactivation (Fig. 17C), and generation of reverse faults. Latite porphyry dikes, Marginal Breccia zones, and pebble dikes were emplaced into dilational cone sheets above the magma chamber. Fluid and/or magmatic pressures associated with the resurgent magma eventually exceeded the lithostatic stress resulting in explosive fragmentation, fluidization, and ultimately formation of the Braden Breccia. This brecciation was possibly phreatomagmatic (e.g., Sillitoe, 1985), although direct evidence for this process (i.e., juvenile clasts) is lacking. The breccia pipe utilized the concentric fractures generated during the Marginal Breccia phase, resulting in the characteristic funnel-shaped Braden Breccia partially bordered by the earlier formed Marginal Breccia (R. Floody, 2000, unpub. report for CODELCO). The Braden Pipe is located close to the center of the deposit, indicating that the locus of the intruding magma and related stresses did not change markedly from the late magmatic and principal hydrothermal stages to the late hydrothermal stage.

During and after these stages of intrusion and withdrawal, minor northeast-trending faults and veins were generated (Fig. 17C) due to movements along the Teniente fault zone. These structures, as well as the north-northwest–northwest trend of the dacite intrusions, are the only features associated with far-field stresses that exceeded localized stresses induced by the intruding magma.

Discussion

Age of mineralization

Re-Os dating of molybdenite using a double Os spike (Stein et al. 2001; Markey et al. 2003) was used to address the age of mineralization at El Teniente. Cannell et al. (2003) and Cannell (2004) presented Re-Os age data generated at Colorado State University for molybdenite samples collected from El Teniente during this study. Our high-precision Re-Os ages range from 5.89 to 4.70 Ma (Fig. 18).

Maksaev et al. (2004) reported nine Re-Os ages for molybdenites from El Teniente (Table 3, Fig. 18) and interpreted five episodes of mineralization (6.30 ± 0.03, 5.60 ± 0.02, 5.01–4.96, 4.89 ± 0.08 to 4.78 ± 0.03, and 4.42 ± 0.02 Ma). These Re-Os ages correlate well with their U-Pb ages for the felsic intrusions and ^{40}Ar-^{39}Ar ages for biotite and sericite (Table 3, Fig. 18). Maksaev et al. (2004) therefore concluded

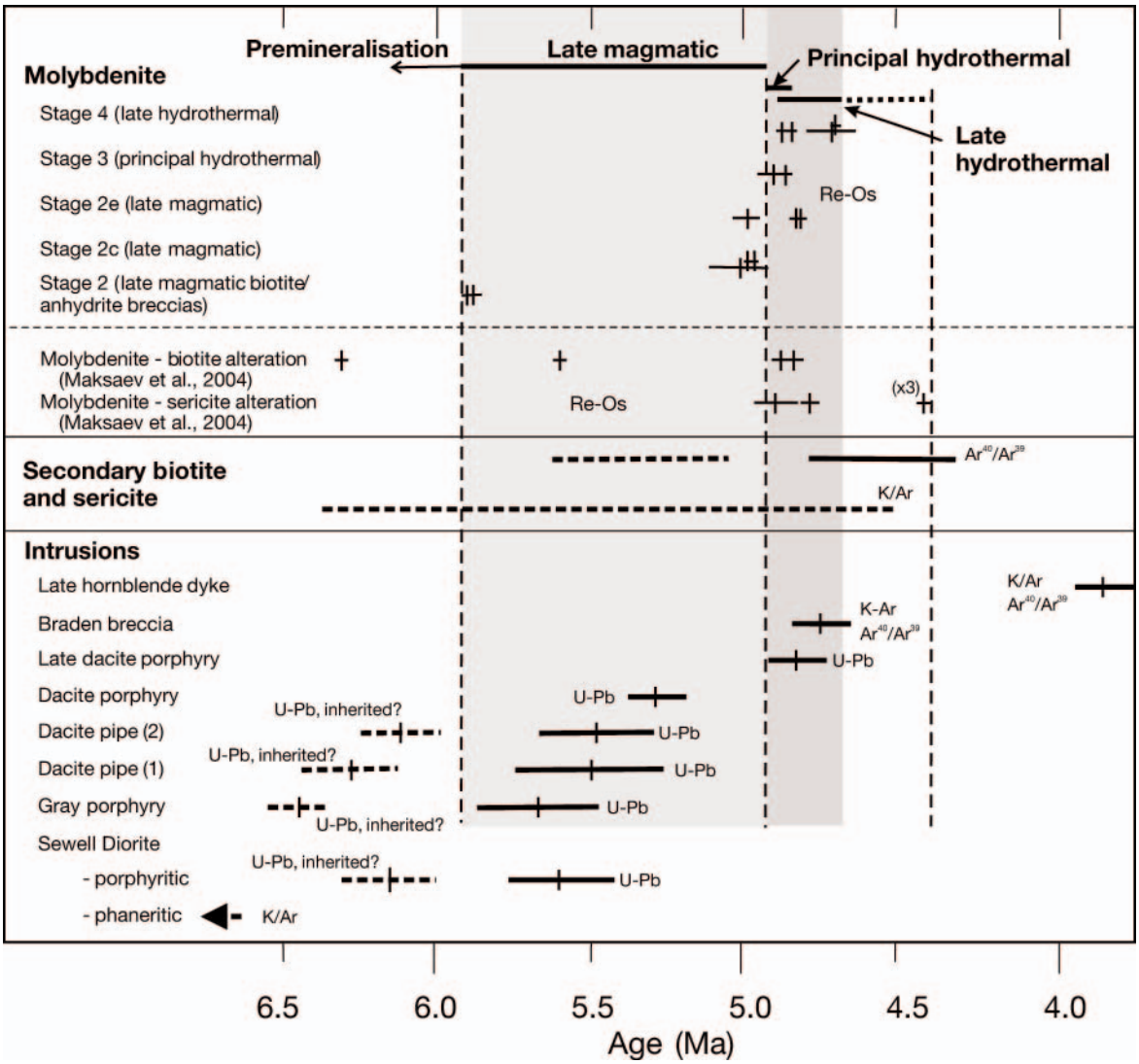

FIG. 18. Summary of geochronological data from El Teniente. Blank-corrected Re-Os ages on molybdenite are from Cannell et al. (2003) and Cannell (2004). Samples are from molybdenite-bearing veins and breccias, some with coexisting chalcopyrite and molybdenite. Errors shown include the uncertainty in the decay constant for ^{187}Re. Other Re-Os data are from Maksaev et al. (2004) as indicated and are not constrained paragenetically, beyond an association with biotite or sericite alteration. U-Pb zircon ages for the intrusions are from Maksaev et al. (2004). Note that the Sewell Tonalite, the gray porphyry, and two samples from the dacite pipes have bimodal age distributions. We have followed the interpretation of Maksaev et al. (2002), whereby the early ages for these four units are inferred to be inherited from previously crystallized zircons, whereas the younger ages represent the ages of final crystallization. This contrasts with the interpretation of Maksaev et al. (2004), who interpreted the older ages to be the intrusion ages and the younger ages to be hydrothermal overgrowths. Biotite and sericite Ar^{40}/Ar^{39} and K-Ar ages are from Maksaev et al. (2004), Cuadra (1986), and P. Cuadra (unpub. report for CODELCO, 1992), respectively. These are significantly younger than the U-Pb and Re-Os ages, due either to resetting during intrusion of the late dacite (Maksaev et al., 2004) or the lower closure temperature of the K/Ar isotope system (Cannell, 2004). The type 2e molybdenite-bearing vein dated at 4.82 to 4.80 Ma may have been reopened, allowing molybdenite precipitation during the principal hydrothermal or late hydrothermal stage, given that the age is significantly younger than the other late magmatic veins. The K-Ar age determination for the phaneritic Sewell diorite is from Cuadra (1986).

that mineralization at El Teniente was sourced directly from the felsic intrusions.

Based on the Re-Os age determinations of Cannell et al. (2003), early-late magmatic vein-hosted molybdenite mineralization is interpreted to have occurred at 5.89 Ma, similar to the youngest U-Pb ages determined for the gray porphyry, the Sewell Tonalite porphyritic phase, and two age determinations from dacite pipes (5.67 ± 0.19, 5.59 ± 0.17, 5.50 ± 0.24, and 5.48 ± 0.19 Ma, respectively, SHRIMP U-Pb zircon data of Maksaev et al., 2002, 2004; Table 3; Fig. 18). Other Re-Os molybdenite ages for the late magmatic stage cluster around 5.0 Ma and are approximately 300,000 yr younger than the dacite porphyry dike (5.28 ± 0.10 Ma: Maksaev et al., 2004). This may be due to the limited number of U-Pb analyses of the multiphase dacite intrusions (i.e., there may be an as yet undated dacitic phase that correlates temporally with

these 5.0 Ma ages). Alternatively, molybdenite mineralization may be related to a deep magma chamber below the level of the mine and was not synchronous with high-level felsic intrusion.

A change to sericite-stable veins of the principal hydrothermal stage occurred at approximately 4.95 to 4.90 Ma (Fig. 18). The principal hydrothermal stage appears to have had a short duration (<100,000 yr) constrained by intrusion of the latite dikes (4.82 ± 0.09 Ma: Maksaev et al., 2004) and the Braden Pipe (Fig. 18).

The late hydrothermal stage mineralization persisted until at least 4.70 Ma (Fig. 18), and some hydrothermal activity persisted until 4.37 ± 0.05 Ma based on $^{40}Ar/^{39}Ar$ and K-Ar dates from Cuadra (1986), P. Cuadra (unpub. report for CODELCO, 1992), and Maksaev et al. (2002, 2004). In total, mineralization, alteration, and cooling of the hydrothermal system at El Teniente spanned at least 1.5 m.y., from 5.9 to 4.4 Ma, coincident with the emplacement of the dacite and latite intrusions (U-Pb ages of 5.7–4.8 Ma: Maksaev et al., 2002, 2004) and the Braden Pipe.

Timing and origin of copper mineralization

Skewes et al. (2002) proposed that copper at El Teniente was initially deposited with widespread brecciation and biotite alteration and was either remobilized or removed by the later intrusive events. Several points from the current study are incompatible with this model. We have observed no textural evidence for the remobilization of early-formed copper sulfides associated with the intrusion of the dacite porphyry. Skewes et al. (2002) argued that the dacite porphyry is low grade compared to the mine andesites because it postdated the biotite breccias and copper mineralization. This study has shown that biotite breccias locally cut the dacites (e.g., Fig. 5C). Furthermore, the low copper grade of the dacite porphyry (a feature common to many porphyry Cu deposits: e.g.; Sillitoe, 2000), may simply reflect its intramineral timing, the presence of, as yet unidentified, late mineral dacite porphyry phases that have diluted grade, or a lack of a suitable physicochemical gradient to precipitate copper or molybdenum in the central, hottest parts of the system. Based on our drill core observations, we conclude that the biotite breccias and associated widespread biotite alteration are temporally and spatially linked to the dacite intrusions and are not a discrete hydrothermal event that preceded dacite emplacement by up to several million years as suggested by Skewes et al. (2002).

Our detailed logging of the mine andesites confirms that breccias, including biotite- and anhydrite-cemented breccias and the Marginal Breccia facies of the Braden Pipe, typically host high-grade ore at El Teniente. However, the breccias are volumetrically minor in comparison to the several cubic kilometers of felsic intrusions and andesitic host rocks that contain the pervasively developed vein stockwork that hosts the bulk of the ore at El Teniente.

Geochronology confirms the findings of Howell and Molloy (1960), Camus (1975), Villalobos (1975), and Cuadra (1986) that the mineralization, veining, and alteration at El Teniente are temporally linked to felsic intrusions. Vein overprinting relationships indicate that the late magmatic stage vein-hosted mineralization overlapped with the multistage dacite intrusions. The dacite pipes, the southern end of the dacite porphyry dike, and the gray porphyry appear to have acted as fluid conduits and focused veining, brecciation, and high-grade mineralization proximal to their contacts. The pervasive alteration assemblages, sulfide assemblages, and the mineralogy and densities of the late magmatic veins all vary systematically, both outward and upward from the dacite porphyry to the periphery of the deposit.

We interpret the predominance of concentric and radial vein orientations in all stages of mineralization at El Teniente to indicate that emplacement of a large pluton below the exposed levels of the mine localized stresses and controlled vein formation throughout the life of the hydrothermal system, from early stages of stockwork development to later stages of brecciation, to form the Braden Pipe. This pluton is interpreted to have sourced both the felsic intrusions and mineralizing fluids. We speculate that episodes of magma intrusion and withdrawal, coupled with decreasing depths and pressures due to tectonic uplift and concomitant erosion (e.g. Kurtz et al., 1997) could account for differences between the three main stages of mineralization at Teniente.

Conclusions

El Teniente is a typical, albeit enormous, Cu-Mo porphyry deposit. It is characterized by multiple phases of weakly to strongly altered felsic intrusions. It has an alteration paragenesis and distribution typical of other porphyry Cu deposits (e.g., Lowell and Guilbert, 1970). Its vein paragenesis is similar to El Salvador (Gustafson and Hunt, 1975). A large, late-stage breccia pipe cuts the mineralization, similar to deposits such as Batu Hijau (Garwin, 2002). Two distinctive features of El Teniente are worthy of note. First, of the 14 vein stages, all but the first two and the last (premineralization stage and type 4d; Table 5) contain Cu-Fe sulfides, indicating that during every paragenetic stage copper was carried in the fluid, and conditions existed to cause precipitation of Cu-bearing sulfides from the fluids. Second, despite the location of El Teniente at the intersection of two district- to regional-scale fault zones, far-field stresses do not appear to have influenced vein development. Instead we suggest that stresses localized above a deep-seated magma body produced the observed vein array and influenced resurgence and withdrawal of magma.

Our interpreted geologic evolution of El Teniente is summarized as follows. The deposit formed during the final stages of a prolonged period of intrusive activity within a Miocene-Pliocene magmatic arc (e.g., Kay et al., 1999; Charrier et al., 2002). Volcanic and volcaniclastic rocks of the Farellones Formation were intruded by a mafic to intermediate sill-stock complex approximately 11 to 9 Ma. This was followed by intrusion of the Sewell Tonalite (part of a 9–7 Ma intrusive complex), which was associated with minor premineralization-stage alteration and veining.

During the latest Miocene, a large, deep-seated, felsic pluton was emplaced. Fluid exsolution from the crystallizing pluton led to the formation of abundant mineralized late magmatic stage veins and lesser biotite-cemented breccias, together with widespread biotite alteration of the wall-rock package. The parent pluton controlled stresses in the deposit (Fig. 18A) and was the source for high-level felsic intrusions dated between 5.7 and 5.3 Ma (Maksaev et al., 2002, 2004).

Late magmatic-stage mineralization continued until approximately 4.95 to 4.90 Ma and was followed by the short lived (<100,000 yr) principal hydrothermal stage. During the principal hydrothermal stage chalcopyrite-rich veins with phyllic halos were emplaced, which host approximately 30 percent of Teniente's copper resource.

Relaxation of the magma-induced stresses led to a stage of subsidence, possibly due to withdrawal of the magma chamber (Fig. 17B). As a result, steeply dipping concentric veins and normal faults formed during the late hydrothermal stage. Latite porphyries and the Braden Pipe were emplaced approximately 4.8 Ma (Fig. 17C), associated with further late hydrothermal-stage veining and alteration. Explosive brecciation and formation of the Braden Breccia apparently depressurized the parent pluton and terminated igneous activity. Mostly late stage northeast-trending faults and minor mineralized veins formed due to movements along the Teniente fault zone (Fig. 17C). The waning stages of the hydrothermal system continued until approximately 4.4 Ma. The last stage in the evolution of El Teniente was intrusion of thin postmineralization lamprophyre dikes at 3.8 Ma.

Acknowledgments

This work was conducted as part of the senior author's Ph.D. dissertation at the University of Tasmania, which was part of the Australian Mineral Industry Research Assocation (AMIRA)-funded Giant Ore Deposits Systems project (P511). We thank all of the other members of the P511 research team, particularly Peter Hollings, Peter Frikken, Glen Masterman, Paul Gow, and Gem Midgley, our AMIRA industry sponsors, and also the AMIRA research coordinator, Joe Cucuzza. The senior author received an Australian Research Council (ARC) APA-I postgraduate research scholarship, which is gratefully acknowledged. We also thank the ARC for additional funding through the Special Research Centre and Linkage grant schemes. The Re-Os work was funded by NSF grant EAR-0087483 (H Stein). Supintendencía de Geología El Teniente, CODELCO-Chile, and CODELCO Central are thanked for providing additional financial and logistical support. Francisco Camus and Jorge Skármeta are thanked for organizing access to El Teniente and for their support and helpful discussions. Patricio Zuñíga, Ricardo Floody, Rodrigo Morel, and all of the other geologists and engineers from El Teniente, and also Alex Losada, Ron Berry, and Jocelyn McPhie are thanked for many useful conversations and for their assistance onsite. Thanks to reviewers R. Tosdal, R. Sillitoe, and A. Skewes, and also to M. Hannington, for their detailed critiques of the paper and comments that have helped to improve the quality of this manuscript.

August 4, 2004; July 15, 2005

REFERENCES

Acocella, V., Cifelli, F., and Funiciello, R., 2000, Analogue models of collapse calderas and resurgent domes: Journal of Volcanology and Geothermal Research, v. 104, p. 81–96.

Atkinson, W.W., Souviron, S., Vehrs, T.I., and Faunes, A., 1996, Geology and mineral zoning of the Los Pelambres porphyry Cu deposit, Chile: Society of Economic Geologists Special Publication 5, p. 131–155.

Burnham, C.W., 1979, Magmas and hydrothermal fluids, *in* Barnes, H.L., ed., Geochemistry of hydrothermal ore deposits: New York, Wiley-Interscience, p. 71–136.

Camus, F., 1975, Geology of the El Teniente orebody with emphasis on wallrock alteration: Economic Geology, v. 70, p. 1341–1372.

Camus, F., 2002, The Andean porphyry systems: Hobart, Tasmania, University of Tasmania, CODES Special Publication 4, p. 1–38.

Cannell, J., 2004, El Teniente porphyry copper-molybdenum deposit, central Chile: Unpublished Ph.D. thesis, Hobart, University of Tasmania, 317 p.

Cannell, J., Cooke, D.R., Stein, H.J., and Markey, R.J., 2003, New paragenetically constrained Re-Os molybdenite ages for El Teniente Cu-Mo porphyry deposit, central Chile [abs]: Society for Geology Applied to mineral Deposits (SGA), Athens, 2003, Abstracts with Programs, v. 1, p. 255–258.

Charrier, R., Baeza, O., Elgueta, S., Flynn, J.J., Gans, P., Kay, S.M., Munoz, N., Wyss, A.R., and Zurita, E., 2002, Evidence for Cenozoic extensional basin development and tectonic inversion south of the flat-slab segment, southern central Andes, Chile (33°–36°S.L.): Journal of South American Earth Sciences, v. 15, p. 117–139.

Cuadra, P., 1986, Geocronología K-Ar del yacimiento El Teniente y areas adyacentes: Revista Geológica de Chile, v. 27, p. 3–26.

Duarte, P.O., 2000, Caracterización geológica y geotécnica del pórfido dacitico El Teniente: Unpublished Honours thesis, Santiago, Universidad de Chile, 80 p.

Engel, A.E., and Engel, C.G., 1960, Progressive metamorphism and granitization of the major paragneiss, northwest Adirondack Mountains, New York: Geological Society of America Bulletin, v. 71, p. 1–57.

Faunes, A., 1981, Caracterización de la mineralogía metalica y alteración en un sector del Stock Tonalitico del yacimiento El Teniente: Unpublished Honours thesis, Santiago, Universidad de Chile, 175 p.

Garrido, I., Riveros, M., Cladouhos, T., Espineira, D., and Allmendinger, R., 1994, Modelo geológico estructurál del yacimiento El Teniente: Congreso Geológico Chileno, 7th, Concepción, 1994, Actas, v. 2, p. 1553–1558.

Garwin, S., 2002, The geological setting of intrusion-related hydrothermal systems near the Batu Hijau porphyry Cu-Au deposit, Sumbawa, Indonesia: Society of Economic Geologists Special Publication 9, p. 333–366.

Godoy, E., Yañez, G., and Vera, E., 1999, Inversion of an Oligocene volcanotectonic basin and uplifting of its superimposed Miocene magmatic arc in the Chilean Central Andes: First seismic and gravity evidences: Tectonophysics, v. 306, p. 217–236.

Gustafson, L.B., and Hunt, J.P., 1975, The porphyry copper deposit at El Salvador, Chile: Economic Geology, v. 70, p. 857–912.

Guzman, C.G., 1991, Alteración y mineralización de los Pórfidos Dioriticos del sector centrál, yacimiento El Teniente: Unpublished honours thesis, Santiago, Universidad de Chile, 143 p.

Heidrick, T.L., and Titley, S.R., 1982, Fracture and dike patterns in Laramide plutons and their structural and tectonic implications; American Southwest, *in* Titley S.R., ed., Advances in geology of porphyry Cu deposits, southwestern North America: Tucson, University of Arizona Press, p. 73–91.

Holliday, J.R., Wilson, A.J., Blevin, P.L., Tedder, I.J., Dunham, P.D., and Pfitzner, M., 2002, Porphyry Au-copper mineralization in the Cadia district, eastern Lachlan fold belt, New South Wales, and its relationship to shoshonitic magmatism: Mineralium Deposita, v. 37, p. 100–116.

Howell, F.H., and Molloy, J. S., 1960, Geology of the Braden orebody, Chile, South America: Economic Geology, v. 55, p. 863–905.

Kay, S.M., and Kurtz, A., 1995, Magmatic and tectonic characterization of the El Teniente region: Internal report, Superintendencía de Geología, El Teniente, CODELCO, 180 p.

Kay, S., Mpodozis, C., and Coira, B., 1999, Neogene magmatism, tectonism, and mineral deposits of the central Andes (22° to 33° latitude): Society of Economic Geologists Special Publication 7, p. 27–59.

Kirkham, R.V., and Sinclair, W.D., 1988, Comb quartz layers in felsic intrusions and their relationship to porphyry deposits: Canadian Institute of Mining and Metallurgy, v. 39, p. 50–71.

Koide, H., and Bhattacharji, S., 1975, Formation of fractures around magmatic intrusions and their role in ore localization: Economic Geology, v. 70, p. 781–799.

Kurtz, A., Kay, S.M., Charrier, R., and Farrar, E., 1997, Geochronology of Miocene plutons and exhumation history of the El Teniente region, central Chile (34–35ºS): Revista Geológica de Chile, v. 24, p. 75–90.

Le Bel, L., 1979, Magmatic and hydrothermal micas in the environment of the Cerro Verde-Santa Rosa porphyry Cu, Peru, *in* Robert, J. L., ed., Les Micas; Chimie et cristallochimie: Paris, Masson, p. 35–41.

Lindgren, W., and Bastin, E.S., 1922, Geology of the Braden mine, Rancagua, Chile: Economic Geology, v. 17, p. 863–905.

Lindsay, D.D., Zentilli, M., and Rojas de la Rivera, J., 1995, Evolution of an active ductile to brittle shear system controlling mineralization at Chuquicamata porphyry copper deposit, northern Chile: International Geology Reviews, v. 37, p. 945–958.

Lowell, D., and Guilbert, J.M., 1970, Lateral and vertical alteration-mineralization zoning in porphyry ore deposits: ECONOMIC GEOLOGY, v. 65, p. 373–408.

Maksaev, V., Munizaga, F., McWilliams, M., Fanning, M., Mathur, R., Ruiz, J., and Thiele, K., 2002, El Teniente porphyry Cu deposit in the Chilean Andes: New geochronological time frame and duration of hydrothermal activity [abs]: Geological Society of America Abstracts with Programs, v. 34, no. 6, p 336.

Maksaev, V., Munizaga, F., McWilliams, M., Fanning, M., Mathur, R., Ruiz, J., and Zentilli, M., 2004, New chronology for El Teniente, Chilean Andes, from U-Pb, $^{40}Ar/^{39}Ar$, Re-Os, and fission-track dating: Implications for the evolution of a supergiant porphyry Cu-Mo deposit: Society of Economic Geologists Special Publication 11, p. 15–54.

Ossandón, G., 1974, Petrografía y alteración del Pórfido Dacitico, yacimiento El Teniente: Unpublished honours thesis, Santiago, Universidad de Chile, 112 p.

Reich, M.H., 2000, Estudio petrográfico, mineraloquímico y geoquímico de los cuerpos intrusivos de Sewell y La Huifa en el sector del yacimiento El Teniente, VI Región, Chile: Unpublished Honours thesis, Concepción, Universidad de Concepción, 95 p.

Rivera, O., and Cembrano, J., 2000, Modelo de formación de cuencas volcano-tectónicas en zonas de transferencia oblicuas a la cadena Andina: el caso de las cuencas Oligo-Miocenos de Chile central y su relación con estructuras WNW-NW (33°00'-34°30' LS) [abs]: Congresso Geológico Chileno, 9th, Puerto Varas, Chile, 2000, Actas, 5 p.

Rivera, O., and Falcón, M., 2000, Las Formaciones Farellones, Coya-Machalí y Abanico en los aldredores del yacimiento El Teniente: Sequencias de cuencas volcano-tectonicas transversales del Oligo-Mioceno de Chile central (33°45'-34°30' LS): Congresso Geológico Chileno, 9th, Puerto Varas, Chile, 2000, Actas, 5 p.

Riveros, M., 1989, Geología del pórfido latitico sector sur yacimiento El Teniente: Unpublished Honours thesis, Santiago, Universidad de Chile, 133 p.

Rojas, A., 2002, Petrografía y geoquímica del pórfido dacitico Teniente, yacimiento El Teniente, Provincia de Cachapoal, VI Región, Chile: Unpublished Honours thesis, Concepción, Universidad de Concepción, 118 p.

Rytuba, J.J., 1994, Evolution of volcanic and tectonic features in caldera settings and their importance in localization of ore deposits: ECONOMIC GEOLOGY, v. 89, p. 1687–1696.

Serrano, L., Vargas, R., Stambuk, V., Aguilar, C., Galeb, M., Holmgren, C., Contreras, A., Godoy, S., Vela, I., Skewes M.A., and Stern C.R., 1996, The late Miocene to early Pliocene Rio Blanco-Los Bronces copper deposit, Central Chilean Andes: Society of Economic Geologists Special Publication 5, p. 119–130.

Shannon, J.R., Walker, B.M., Carten, R.B., and Geraght, E.P., 1982, Unidirectional solidification textures and their significance in determining relative ages of intrusions at the Henderson mine, Colorado: Geology, v. 10, p. 293–297.

Sillitoe, R.H., 1985, Ore-related breccias in volcanoplutonic arcs: ECONOMIC GEOLOGY, v. 80, p. 1467–1514.

——2000, Gold-rich porphyry deposits: Descriptive and genetic models and their role in exploration and discovery: Reviews in Economic Geology, v. 13, p. 315–345.

Skewes, A., Arévalo, A., Floody, R., Zúñiga, P.H., and Stern, C.R., 2002, The giant El Teniente breccia deposit: Hypogene copper distribution and emplacement: Society of Economic Geologists Special Publication 9, p. 299–332.

Thiele, R., Beccar, I., Levi, B., Nystrom, J., and Vergara, M., 1991, Tertiary Andean volcanism in a caldera-graben setting: Geologische Rundschau, v. 80, p. 179–186.

Titley, S.R., 1990, Evolution and style of fracture permeability in intrusion-centered hydrothermal systems, *in* Titley S.R., ed., The role of fluids in crustal processes: Washington DC, National Acadamic Press, p. 50–63.

Tosdal, R.M., and Richards, J.P., 2001, Magmatic and structural controls on the development of porphyry Cu ± Mo ± Au deposits: Reviews in Economic Geology, v. 14, p. 157–181.

Villalobos, J., 1975, Alteración hidrotermal en las andesitas del yacimiento El Teniente, Chile: Unpublished Ph.D. thesis, Santiago, Universidad de Chile, 125 p.

Zúñiga, P., 1982, Alteración y mineralización hipógenas en el sector oeste del yacimiento El Teniente: Unpublished Honours thesis, Santiago, Universidad de Chile, 107 p.